Development 136, 1951-1960 (2009) doi:10.1242/dev.031369

Potential hepatic stem cells reside in EpCAM$^+$ cells of normal and injured mouse liver

Mayuko Okabe[1,*], Yuko Tsukahara[1,*], Minoru Tanaka[1,*,†], Kaori Suzuki[1], Shigeru Saito[1], Yoshiko Kamiya[1], Tohru Tsujimura[2], Koji Nakamura[3] and Atsushi Miyajima[1]

Hepatic oval cells are considered to be facultative hepatic stem cells (HSCs) that differentiate into hepatocytes and cholangiocytes in severely injured liver. Hepatic oval cells have also been implicated in tumorigenesis. However, their nature and origin remain elusive. To isolate and characterize mouse oval cells, we searched for cell surface molecules expressed on oval cells and analyzed their nature at the single-cell level by flow cytometric analysis and in the in vitro colony formation assay. We demonstrate that epithelial cell adhesion molecule (EpCAM) is expressed in both mouse normal cholangiocytes and oval cells, whereas its related protein, TROP2, is expressed exclusively in oval cells, establishing TROP2 as a novel marker to distinguish oval cells from normal cholangiocytes. EpCAM$^+$ cells isolated from injured liver proliferate to form colonies in vitro, and the clonally expanded cells differentiate into hepatocytes and cholangiocytes, suggesting that the oval cell fraction contains potential HSCs. Interestingly, such cells with HSC characteristics exist among EpCAM$^+$ cells of normal liver. Intriguingly, comparison of the colony formation of EpCAM$^+$ cells in normal and injured liver reveals little difference in the number of potential HSCs, strongly suggesting that most proliferating mouse oval cells represent transit-amplifying cells rather than HSCs.

KEY WORDS: Hepatic stem cell, Oval cell, EpCAM, TROP2 (TACSTD2), Hepatocyte, Cholangiocyte, Liver injury

INTRODUCTION

Most of the metabolic functions in the liver are carried out by hepatocytes that form hepatic cords, whereas cholangiocytes form bile ducts that drain bile produced by hepatocytes. During development, hepatocytes and cholangiocytes, two types of hepatic epithelial cells, derive from hepatoblasts emerging from the foregut endoderm (Notenboom et al., 2003; Zaret, 2000). Hepatoblasts are highly proliferative and express hepatocytic proteins such as albumin (ALB) and alpha-fetoprotein (AFP), an immature hepatocyte marker. As the liver develops, hepatoblasts propagate and those close to the portal mesenchyme differentiate into cholangiocytes, while the rest become mature hepatocytes (Lemaigre, 2003). Therefore, hepatoblasts are thought to be hepatic stem/progenitor cells in the fetus.

By contrast, it is highly controversial whether adult mammalian liver contains hepatic stem cells (HSCs). Adult liver has a remarkable potential to regenerate from severe parenchymal loss, even though hepatocytes and cholangiocytes are mitotically dormant under normal conditions. Hepatocytes have a remarkable potential to self-replicate (Fausto, 2004; Michalopoulos and DeFrances, 1997) and are capable of at least 80 doublings by serial transplantation (Overturf et al., 1997), allowing the liver to regenerate. However, liver injury that limits this pathway accompanies the proliferation of a potential stem/progenitor cell compartment at the interface of the biliary tree and hepatic cords, which is known as the ductular reaction (Alison et al., 1996; Roskams et al., 2004; Theise et al., 1999). These undifferentiated epithelial cells are often referred to as 'oval cells' because of their ovoid nucleus (Farber, 1956). Upon activation, oval cells expand into liver parenchyma from the portal area. Oval cells express both ALB and cytokeratin 19 (CK19; KRT19 – Mouse Genome Informatics), which are hepatocytic and cholangiocytic markers, respectively, and are believed to differentiate into hepatocytic and biliary lineages, similar to hepatoblasts in embryonic liver. Thus, oval cells are thought to be facultative stem/progenitor cells in adult liver. Although oval cells have been most extensively studied in rodents, similar cells have been found in connection with various human liver diseases and are implicated in tumorigenesis (Fausto, 2004; Lee et al., 2006). Whether oval cells constitute HSCs has been debated in numerous reports involving various rodent injury models using chemical reagents, including carcinogenic agents. The 2-acetylaminofluorene (2-AAF)/partial hepatectomy (PH) model, in which hepatocyte proliferation is blocked by 2-AFF prior to PH, has been extensively used to characterize oval cells in rats (Evarts et al., 1987; Laishes and Rolfe, 1981). However, the same procedure does not generate oval cells in mice and alternatives such as the use of a choline-deficient ethionine-supplemented diet (Akhurst et al., 2001) and a 3,5-diethoxycarbonyl-1,4-dihydro-collidine (DDC)-containing diet (Preisegger et al., 1999; Wang et al., 2003) have been developed. Although the proliferating epithelial cells that are present in the periportal region upon injury caused by various insults are referred to as oval cells, it remains unclear whether oval cells generated via different protocols in different species have the same characteristics. A major problem in characterizing oval cells is the lack of appropriate cell surface markers to identify and isolate the oval cell compartment. Therefore, despite a large number of studies, the exact nature of oval cells – including their origin, stemness and bi-directional differentiation – is still poorly understood. Because of the difficulty in performing clonal analysis of HSCs, it has also been unclear whether HSCs exist in normal liver.

The aim of this study was to identify cell surface molecules on mouse oval cells and to analyze their nature at the clonal level. To this end, we utilized the 2-AAF/PH rat model and the DDC diet

[1]Laboratory of Cell Growth and Differentiation, Institute of Molecular and Cellular Biosciences, The University of Tokyo, Tokyo 113-0032, Japan. [2]Department of Pathology, Hyogo College of Medicine, Nishinomiya, Hyogo 663-8501, Japan. [3]LivTech, Miyamae-ku, Kawasaki, Kanagawa 216-0001, Japan.

*These authors contributed equally to this work
†Author for correspondence (e-mail: tanaka@iam.u-tokyo.ac.jp)

Accepted 31 March 2009

mouse model to generate oval cells and found that epithelial cell adhesion molecule (EpCAM) and the related molecule, TROP2 (TACSTD2), were upregulated in these livers. EpCAM was expressed in normal cholangiocytes and also in oval cells in the liver of mice fed the DDC diet (DDC liver). By contrast, TROP2 was expressed in almost all EpCAM$^+$ cells in DDC liver, but not in normal liver, indicating that TROP2 is a novel marker to distinguish between normal cholangiocytes and oval cells. Furthermore, we isolated EpCAM$^+$ cells from DDC liver and demonstrated that clonally expanded cells were able to differentiate into hepatocytes and cholangiocytes. Finally, we provide evidence for the presence of potential HSCs in EpCAM$^+$ cells of normal liver and compare their characteristics before and after oval cell activation.

MATERIALS AND METHODS

Animals

C57BL/6 mice (Japan SLC, Hamamatsu, Japan) at 8-12 weeks were used for all experiments. All experiments with animals were performed according to institutional guidelines. The diet containing 0.1% DDC was purchased from CLEA, Japan. Mouse oval cells were activated by feeding with the diet containing 0.1% DDC.

Identification of cDNA encoding a membrane protein

Total RNA was prepared from the non-parenchymal fraction of rat liver treated with 2-AAF/PH at 7 days after PH as described previously (Tanimizu et al., 2004b). Total RNA was amplified using the MessageAmp aRNA Amplification Kit (Ambion), and used to construct a cDNA library in the pMXs-SST vector using the SuperScript Choice System (Invitrogen, Carlsbad, CA, USA). The cDNA library contained 4.3×10^6 independent clones. The signal sequence trap method was performed as described previously (Kojima and Kitamura, 1999).

Preparation of liver cells and flow cytometry (FCM)

A single-cell suspension from DDC and normal livers was obtained by a modified two-step collagenase perfusion method as described previously (Seglen, 1976). In short, livers were perfused with liver perfusion medium (Invitrogen) at a flow rate of 3 ml/minute for 5 minutes. Then, the liver was perfused with basic perfusion solution (136 mM NaCl, 5.4 mM KCl, 5 mM $CaCl_2$, 0.5 mM NaH_2PO_3 $2H_2O$, 0.42 mM Na_2HPO_3 $12H_2O$, 10 mM HEPES pH 7.5, 5 mM glucose and 4.2 mM $NaHCO_3$) containing 0.5 g/l collagenase type IV (Sigma, St Louis, MO, USA) at a flow rate of 3 ml/minute for 8 minutes. The digested liver was transferred to a glass dish and chopped into small pieces using a surgical knife in D-PBS (Dulbecco's phosphate-buffered saline). Cells dispersed by pipetting were passed through a 70-μm cell strainer and the flow-through fraction was used for the next step as the first cell suspension. The undigested clot on the strainer was recovered and redigested with basic perfusion solution containing 0.5 g/l collagenase type IV, 0.5 g/l pronase (Roche Diagnostics) and 50 mg/l DNase I (Sigma) by stirring for 20 minutes at 37°C. This digested liver was also passed through a 70-μm cell strainer and the flow-through fraction was combined with the first cell suspension. After centrifugation at 700 rpm (100 *g*) for 2 minutes, the supernatant was transferred to a new tube and the centrifugation repeated until no cell pellet was visible. The final supernatant was centrifuged at 1200 rpm (300 *g*) for 5 minutes and the precipitated cells were used as non-parenchymal cells (NPCs) for FCM analysis. Aliquots of cells were blocked with anti-FcR antibody, co-stained with fluorescein- and biotin-conjugated antibodies, washed, incubated with allophycocyamin-conjugated streptavidin (Invitrogen), and analyzed by FACSCalibur (Becton Dickinson). Dead cells were excluded by propidium iodide staining.

Antibodies and immunohistochemistry (IHC)

The anti-EpCAM monoclonal antibody was generated by immunization of a rat with a Ba/F3 cell transfectant overexpressing EpCAM cDNA. The establishment of hybridoma clones was performed as described previously (Hara et al., 1999). The anti-EpCAM monoclonal antibody was biotinylated using Amersham ECL Protein Biotinylation Module (GE Healthcare, UK) or fluorescein-conjugated using the Fluorescein Labeling Kit-NH_2 (Dojindo Molecular Technologies), and then used for all FCM analyses. The rabbit anti-mouse CK19 polyclonal antibody was raised against the C-terminal peptide, HYNNLPTPKAI, and the serum was used for IHC as previously described (Tanimizu et al., 2003). The biotin-conjugated anti-mouse TROP2 antibody was purchased from R&D Systems. The anti-human Ki67 antibody was purchased from Becton Dickinson. Frozen sections (8 μm) of livers were prepared using a HM505E cryostat (Microm International) after fixation with 4% paraformaldehyde, and incubated with each antibody, followed by a biotin- or fluorescein-conjugated secondary antibody. The signals were visualized by fluorescence microscopy.

RNA extraction and reverse transcription PCR (RT-PCR)

Total RNA was extracted from each cell preparation using Trizol reagent (Invitrogen). Total RNA (1 μg) and random hexamer primers were used to synthesize cDNA using the First-Strand cDNA Synthesis Kit (Amersham Pharmacia Biotech). The samples were denatured at 94°C for 5 minutes, then subjected to 25-40 cycles of denaturation at 94°C for 30 seconds, annealing at 52-57°C for 30 seconds, and extension at 72°C for 1 minute, with the final extension at 72°C for 5 minutes. PCR primers for mouse genes are shown in Table 1. The quantitative real-time RT-PCR was performed using a LightCycler ST300 (Roche) and the following primers (5′ to 3′): rat *Epcam*, TCTACAAGGAAGAGATCAGCAAAA and TGTGTATC-TCACCCATCTCCTTT; rat *Trop2*, GACCAAATGTGTTGGCCTGT and GTCACAGCTGGGAGGAAAAT; rat *Hprt*, GACCGGTTCTGT-CATGTCG and ACCTGGTTCATCATCACTAATCAC.

Table 1. Oligonucleotides used in RT-PCR

Gene	Forward (5′ to 3′)	Reverse (5′ to 3′)
Epcam	CGGCTCAGAGAGACTGTGTC	GATCCAGTAGGTCCTCACGC
Ck19	GTCCTACAGATTGACAATG	CACGCTCTGGATCTGTGACAG
Ck7	GGGATGACCTCCGCAACACC	CTCCAGCAGCTTGCGGTAGG
Alb	CATGACACCATGCCTGCTGAT	GCCTTTCCACCAGGGATCCAC
Afp	CTGGAGTGTCTGCAGGATGG	CCACAGCCGGACCATTTCTC
Gapdh	GGAGCGAGACCCCACTAA	GTGTAGCCCAAGATGCCC
Hprt	GACTGAAAGACTTGCTCGAG	CCAGCAAGCTTGCAACCTTAACAA
G6Pase	AACCCATTGTGAGGCCAGAGG	TACTCATTACACTAGTTGGTC
Tat	TGCATCCTCCTGAAGACATG	CTTCTCTCTGGTGTAGCTCT
Cps	ACTGAGAGATGCTGACCCTA	CCTGGAAATTGGTGAGGAGA
integrin β4	GACCTATGAAGAAGGTGCTC	GGCTCAGATGCGTGCCATAG
Ggt1	GCTGAGCTGATTGAGCATCCG	GGTTGATGAAGTTGGGCGAGC
mucin 1	GAGCGCCAGCCTTGAGTTTG	GGAGGCACTACTGTGGACTG
Trop2	CTGACCTAGACTCCGAGCTG	CCAACCCATCTGGTCTGAGG
claudin 4	GACTTTGACCCCTGCAGAGG	GGCCACAGGCTGTTATGAGC
Cd44	CAGAGGCGACTAGATCCCTC	GAGTCACAGTGCGGGAACTC
Slc10a1	AGATCAAGGCTCACTTCTGG	AGAAGTCCTTCTGCAAGCTG
Tdo2	ACAATGAAGAAGACAGAGC	TGTAGTCTCCTCCAAAGTTA

Culture of EpCAM$^+$ cells and colony formation assay

NPCs were prepared as described above. EpCAM$^+$ cells were sorted by FACSVantage SE (Becton Dickinson). The cells were suspended in the standard medium (Williams' medium E containing 10% FBS, 10 mM nicotinamide, 2 mM L-glutamine, 0.2 mM ascorbic acid, 20 mM HEPES pH 7.5, 1 mM sodium pyruvate, 17.6 mM $NaHCO_3$, 14 mM glucose, 100 nM dexamethasone, 1× ITS (insulin, transferrin, selenium X) and 50 mg/ml gentamicin) and seeded on a type-I collagen-coated dish. human EGF, human recombinant HGF and mouse IL6 were added to the culture to a final concentration of 10 ng/ml each. After the establishment of cell lines, IL6 was excluded from the culture medium because it was confirmed to have no apparent effect. For colony formation assays, EpCAM$^+$ cells were sorted by a two-step selection (see Fig. S1 in the supplementary material) and plated at 1×10^4 cells per 35-mm dish. The isolated cells were cultured for 9 days and then the number and size of colonies were counted.

Differentiation into the hepatocytic lineage in vitro

Clonally expanded cells (3×10^5 per well) were cultured in the standard culture medium in a 6-well plate. After 2 days, 20 ng/ml Oncostatin M (OSM) and 1% DMSO were added into the confluent culture. After 5 days, the medium was changed to standard culture medium containing 20 ng/ml OSM, 1% DMSO and 17% Matrigel (growth factor reduced). After 3 and 5 days, the cultured cells were used for RNA preparation and periodic acid-Schiff (PAS) staining as described (Kamiya et al., 1999).

In vitro differentiation into the cholangiocytic lineage

Cellmatrix Type I-A (Nitta Gelatin) was used for three-dimensional culture to induce cholangiocytic differentiation according to the manufacturer's instructions. In short, 0.3% Cellmatrix Type I-A, a 5× DMEM containing 250 mg/ml gentamicin, and the reconstitution buffer (0.05 M NaOH, 200 mM HEPES pH 7.5, 262 mM $NaHCO_3$) were mixed at a ratio of 7:2:1. This mixture was mixed with an equal volume of 5×10^4 cells suspended in standard culture medium without dexamethasone and nicotinamide but with human recombinant HGF (20 ng/ml). The cell suspension was poured into a 6-well plate and left at 37°C to form a gel. Then, the culture medium was gently laid onto the gel.

RESULTS

Screening for cell surface markers of oval cells

To identify the cell surface molecules expressed on hepatic oval cells, we utilized the signal sequence trap (SST) method, which can efficiently isolate genes encoding a protein with a signal sequence (Kojima and Kitamura, 1999; Watanabe et al., 2007). As there are several protocols for generating oval cells in rats and mice, the characteristics of oval cells might not be the uniform. We therefore searched for cell surface molecules expressed on oval cells in the two species using different protocols (see Fig. S2 in the supplementary material). To this end, we first constructed an SST cDNA library from non-parenchymal cells (NPCs) of rat liver subjected to 2-AAF/PH treatment and identified 54 membrane proteins (see Table S1 in the supplementary material). First, we compared the expression of their counterpart genes for mouse between normal and DDC liver by RT-PCR, and found that *Epcam*, *Trop2*, mucin 1, claudin 4, *Cd44*, integrin β3, *Lyve1*, *gp130* (*Il6st*) and *Fxyd5* were significantly upregulated in DDC liver relative to normal liver. Chronic liver injury caused by DDC diet induces oval cells in mice, whereas PH and carbon tetrachloride-induced acute hepatitis do not. Next, the expression of the candidate genes was compared by northern blotting among normal liver, DDC liver and models of acute hepatitis, resulting in the identification of six of the nine genes that were specifically upregulated in the DDC liver, but not in the other livers (Fig. 1A). The remaining three genes, *Lyve1*, *gp130* and *Fxyd5*, were upregulated in an acute hepatitis model, suggesting that they might be involved in inflammation (data not shown). Because the expression of EpCAM, mucin 1, CD44 and

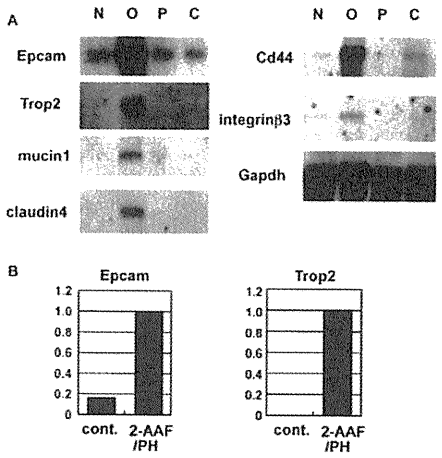

Fig. 1. Expression profiles of candidate genes in normal and injured mouse and rat liver. (**A**) Northern blot analysis of candidate genes in mouse liver. The expression of these genes was selectively upregulated in DDC liver, but not in injured liver without oval cell activation. (**B**) Quantitative RT-PCR of *Epcam* and *Trop2* in rat liver. Whereas *Epcam* was expressed in normal rat liver (cont.) and upregulated in 2-AAF/partial hepatectomy (PH)-treated liver, *Trop2* was not expressed in normal liver but was expressed in 2-AAF/PH-treated liver. N, adult mouse normal liver; O, DDC liver (6 weeks); P, liver 48 hours after 70% PH; C, liver 24 hours after carbon tetrachloride administration.

claudin 4 has been reported to be upregulated in the rat oval cell fraction (Yovchev et al., 2007), the characteristics of mouse oval cells in the DDC model appear similar to those of rat oval cells in the 2-AAF/PH model. In this study, we have focused on two structurally related type-I membrane proteins, EpCAM and TROP2. EpCAM is known to be expressed in many types of normal epithelial cell as well as in tumor cells (Armstrong and Eck, 2003; Went et al., 2004). In the liver, EpCAM is expressed on cholangiocytes but not on hepatocytes (de Boer et al., 1999; Momburg et al., 1987). Consistent with previous studies (Yovchev et al., 2007; Yovchev et al., 2008), real-time PCR showed that *Epcam* was expressed in normal rat liver and its expression was upregulated by 2-AAF/PH (Fig. 1B). As for mouse oval cells, Gleiberman et al. reported that EpCAM is expressed in oval cells upon carbon tetrachloride-induced liver injury (Gleiberman et al., 2005). However, the expression status of EpCAM in DDC liver and the nature of isolated EpCAM$^+$ cells have remained unknown. By contrast, *Trop2* was expressed in both rat and mouse injured liver, but not in normal liver (Fig. 1). TROP2 is a member of the EpCAM family and exhibits nearly 50% homology with EpCAM. TROP2 has been shown to be expressed in various tumors, whereas its expression in the liver was not known. We further examined the expression of EpCAM and TROP2 on mouse oval cells in DDC liver and investigated the nature of isolated EpCAM$^+$ cells.

Expression of EpCAM in mouse hepatic oval cells

As shown in Fig. 2A, after 4 weeks of DDC diet feeding, the mouse liver turned black because of hepatic porphyria resulting from the inhibition of the heme biosynthetic pathway (Fonia et al., 1996). Hematoxylin and Eosin (H&E) staining was performed in adult normal liver and DDC liver. The DDC liver clearly showed numerous small cells with a large nucleus around the portal veins (Fig. 2B). Immunohistochemistry (IHC) for CK19, a marker for oval cells and

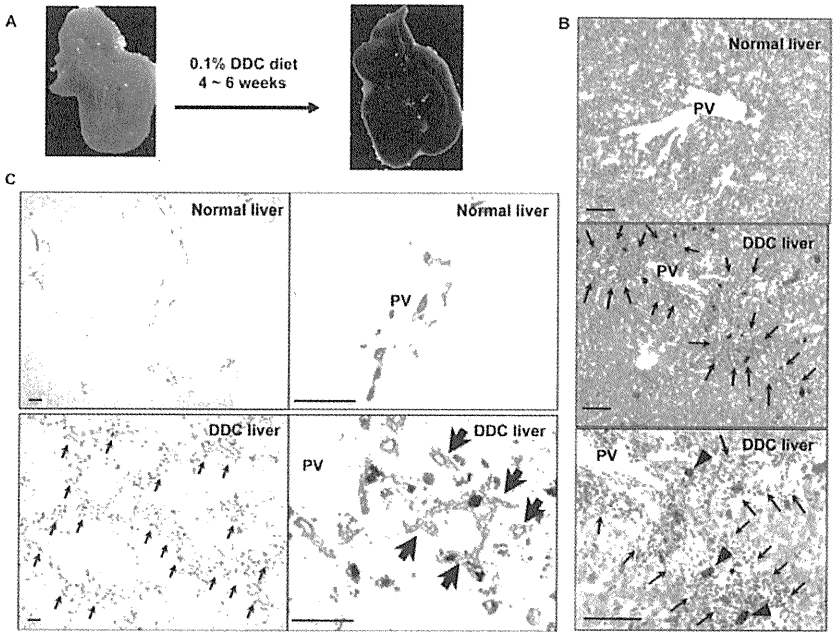

Fig. 2. DDC diet causes hepatic injury and oval cell activation. (**A**) The liver turned black after mice were fed a DDC diet. (**B**) H&E staining of a frozen section of mouse normal liver (top) and 4 weeks after DDC feeding (middle and bottom). Numerous small cells appeared around the portal veins in the DDC liver (arrows). The brown clots represent the deposition of iron hemes (arrowheads). (**C**) Immunohistochemistry (IHC) with anti-CK19 antibody showed that these numerous small cells included CK19-expressing oval cells (arrows) in DDC liver. PV, portal vein. Scale bars: 100 μm

cholangiocytes, demonstrated that these cells included oval cells as well as other CK19-negative cells, such as inflammatory cells and fibroblasts (Fig. 2C). Since EpCAM expression was upregulated in DDC liver, it was examined by IHC using sections of normal liver and of liver from mice fed DDC for 1 or 4 weeks. EpCAM$^+$ bile ducts were located adjacent to the portal vein in normal liver as reported previously (de Boer et al., 1999; Hreha et al., 1999; Joplin et al., 1990), whereas there were many EpCAM$^+$ cells forming ductular structures away from the portal vein in DDC liver (Fig. 3A). IHC with both anti-EpCAM and anti-CK19 antibodies demonstrated that all CK19$^+$ cells expressed EpCAM in DDC liver (Fig. 3B). Thus, all oval cells expressing CK19 also expressed EpCAM. To further investigate the EpCAM$^+$ cells, we generated rat monoclonal antibodies against mouse EpCAM that were applicable for flow cytometry (FCM). FCM of NPCs prepared from DDC liver showed that neither CD45 (PTPRC) nor PECAM was expressed on EpCAM$^+$ cells, indicating that EpCAM$^+$ cells are not hematopoietic or endothelial cells (Fig. 3C). Furthermore, the isolated EpCAM$^+$ cells were individually examined by immunostaining after cytospin. Almost all the sorted cells were immunostained with anti-CK19 antibody as well as A6 antibody, a mouse oval cell marker (Engelhardt et al., 1993) (Fig. 3D). Hepatic oval cells are known to be highly proliferative. To investigate their proliferation in vivo, the isolated EpCAM$^+$ cells were stained with anti-Ki67 antibody (Fig. 3E). Whereas the percentage of Ki67$^+$ cells in the isolated EpCAM$^+$ cells was ~1% in normal liver, it was 12.2% after 1 week on the DDC diet and increased to 17.4% after 4 weeks (Fig. 3F). These results strongly suggested that EpCAM is expressed in proliferating oval cells and that anti-EpCAM antibody is useful for isolating oval cells from mice fed with DDC.

TROP2 is a novel marker for mouse oval cells

Because TROP2 expression was specifically upregulated in both the mouse and rat injury models with oval cell activation (Fig. 1), TROP2 was anticipated to be expressed in oval cells. To reveal TROP2-expressing cells in normal and injured liver, we performed IHC with anti-EpCAM and anti-TROP2 antibodies. In contrast to EpCAM, TROP2 was not expressed in normal mouse liver (Fig. 4A). However, numerous TROP2$^+$ cells appeared around the portal area in DDC liver (Fig. 4B). Double immunostaining of TROP2 and EpCAM clearly showed that most of the EpCAM$^+$ cells co-expressed TROP2 in DDC liver, suggesting that TROP2 is a novel marker for oval cells (Fig. 4B). Although we could not distinguish the original bile duct in DDC liver, almost all EpCAM$^+$ cells expressed TROP2. FCM of the NPCs prepared from DDC liver also showed that the expression level of TROP2 and the population of TROP2$^+$ cells among EpCAM$^+$ cells gradually increased upon ingestion of the DDC diet (Fig. 4C). Consistent with the result of IHC, whereas TROP2 was not present in cholangiocytes expressing EpCAM at day 0, almost all EpCAM$^+$ cells became TROP2$^+$ in the DDC-fed mice and EpCAM$^+$ TROP2$^-$ cells were hardly detected after 4 weeks, suggesting that cholangiocytes themselves might also begin to express TROP2 by oval cell activation in the DDC model. Alternatively, it is also possible that TROP2$^+$ oval cells differentiate into mature cholangiocytes and replace the pre-existing cholangiocytes damaged by DDC administration.

Characterization of mouse oval cells

To reveal the characteristics of mouse oval cells, the gene expression profile of freshly isolated EpCAM$^+$ cells from DDC liver was examined by RT-PCR. As previously reported in rat oval cells, mouse EpCAM$^+$ cells also expressed both cholangiocytic markers [*Ck19*, *Ck7* (*Krt7*) and *Ggt1*] and a hepatocytic marker (*Alb*), whereas the other NPCs did not (Fig. 5A). Consistent with the previous report that AFP expression was rarely detected in mouse oval cells (Jelnes et al., 2007), AFP was not detected in mouse EpCAM$^+$ cells (data not shown). Rat oval cells were reported to express c-KIT, CD34 and THY1 (Petersen et al., 1998). It was also reported that CD133 (PROM1) is expressed in both mouse and rat oval cells (Rountree et al., 2007; Suzuki et al., 2008; Yovchev et al., 2008). Taking advantage of FCM using the anti-EpCAM antibody, we investigated the expression of these oval cell markers in EpCAM$^+$ cells before and after DDC feeding (Fig. 5B) and found

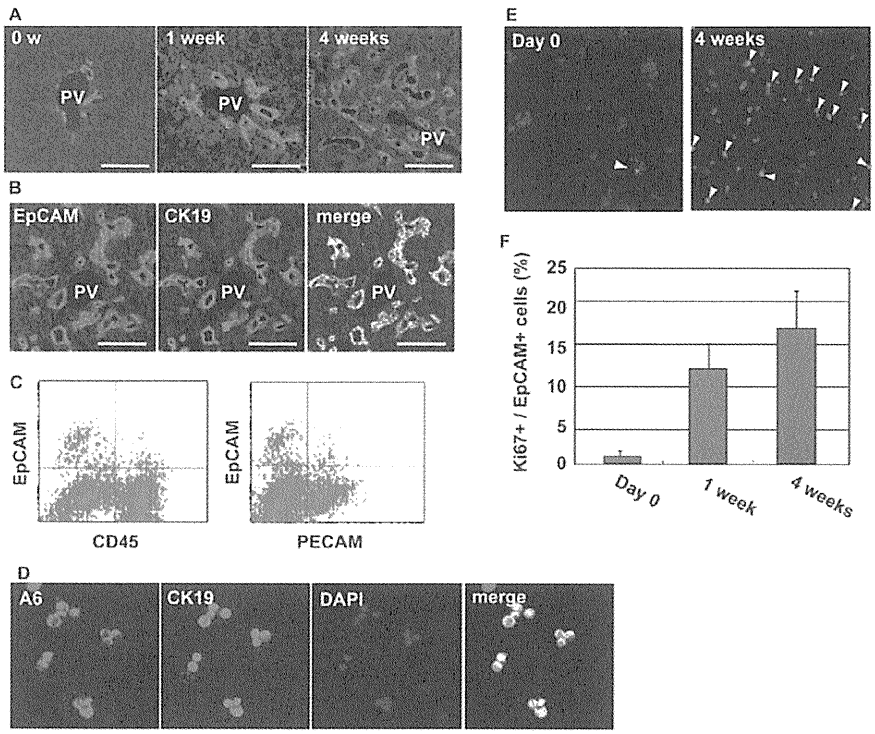

Fig. 3. EpCAM is a cell surface marker for mouse oval cells. (**A**) IHC of frozen liver sections with anti-EpCAM antibody after DDC feeding. EpCAM was expressed in cholangiocytes around the portal vein of normal mouse liver (0 w). Feeding DDC caused the proliferation of EpCAM$^+$ cells (1 and 4 weeks). (**B**) IHC of frozen liver sections with anti-EpCAM and anti-CK19 antibodies after 4 weeks of DDC feeding. (**C**) Flow cytometry (FCM) of non-parenchymal cells (NPCs) prepared from the liver of mice fed DDC for 4 weeks with anti-EpCAM antibody and either CD45 or PECAM antibody. EpCAM$^+$ cells were negative for CD45 (hematopoietic marker) and PECAM (endothelial marker). (**D**) Immunostaining of EpCAM$^+$ cells with anti-A6 and anti-CK19 antibodies by cytospin. EpCAM$^+$ cells expressed both molecules. (**E**) Immunostaining of EpCAM$^+$ cells sorted from normal and DDC liver with anti-Ki67 antibody by cytospin. Many EpCAM$^+$ cells from DDC liver were stained with Ki67 (arrowheads). (**F**) The percentage of Ki67$^+$ cells among EpCAM$^+$ cells after DDC treatment. The data are derived from five different fields of view. Error bars, s.d. PV, portal vein. Scale bars: 100 μm.

that c-KIT, CD34 and THY1 were not expressed in EpCAM$^+$ cells regardless of injury. The expression pattern of CD133 was similar to that of EpCAM, indicating that both molecules are originally expressed in normal cholangiocytes. By contrast, TROP2 was exclusively expressed in oval cells of DDC liver. These results indicate that TROP2 is induced by oval cell activation and that it is a novel marker for oval cells in mice.

Primary culture of EpCAM$^+$ cells from DDC liver

It has been thought that oval cells are proliferative in vivo and possess the potential to differentiate into hepatocytic and cholangiocytic lineages. Therefore, oval cells are considered facultative stem/progenitor cells. To assess such characteristics, we cultured the EpCAM$^+$ cells isolated from DDC liver in vitro. The EpCAM$^+$ cells purified with a cell sorter were seeded onto type-I collagen in the presence of EGF, HGF and IL6. After plating, adherent cells began to proliferate (Fig. 6A) and covered the entire dish after 1 month. The in vitro proliferating EpCAM$^+$ cells were apparently homogeneous and exhibited epithelial cell morphology even after serial passages (Fig. 6B). They could grow and survive for more than 6 months, maintaining a homogenous morphology. These results suggested that EpCAM$^+$ cells derived from DDC liver include cells with high proliferative potential.

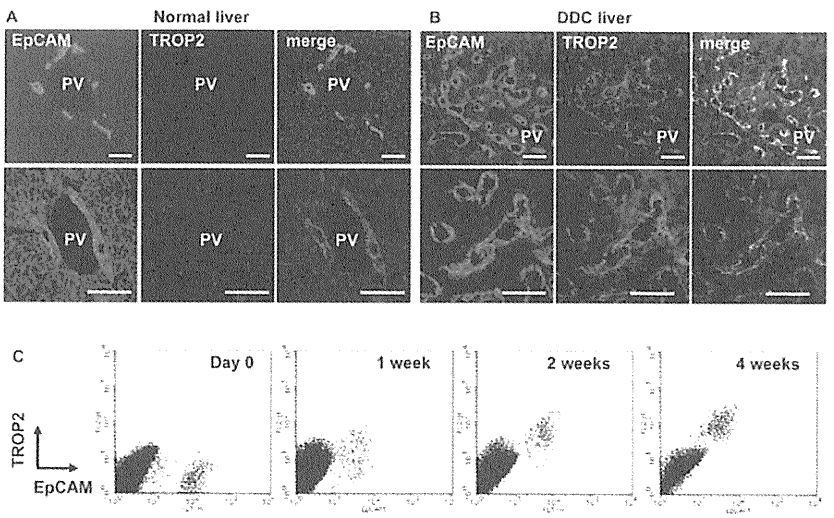

Fig. 4. Expression of EpCAM and TROP2 in normal and injured mouse liver. (**A**,**B**) IHC of frozen sections of normal liver (A) and the liver of mice fed DDC for 5 weeks (B) with anti-EpCAM and anti-TROP2 antibodies. TROP2 was expressed in oval cells but not in normal cholangiocytes. (**C**) FCM of NPCs with anti-EpCAM and anti-TROP2 antibodies after DDC feeding. TROP2 begins to be expressed in EpCAM$^+$ cells as DDC feeding proceeds. PV, portal vein. Scale bars: 100 μm.

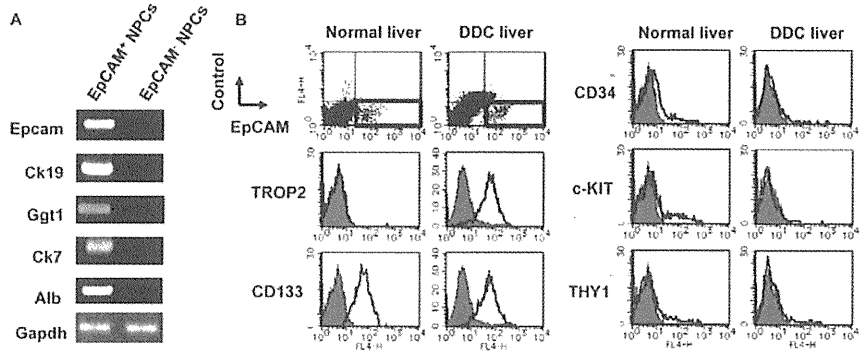

Fig. 5. Characterization of freshly isolated EpCAM⁺ cells. (**A**) RT-PCR of freshly isolated EpCAM⁺ and EpCAM⁻ cells from the liver of mice fed DDC for 4 weeks. NPCs from DDC liver were divided into EpCAM⁺ and EpCAM⁻ cells by FACSVantage, then RT-PCR was performed. (**B**) FCM of EpCAM⁺ cells from normal and DDC livers with known oval cell markers. EpCAM⁺ cells surrounded by bold lines were reanalyzed with other antibodies (TROP2, CD133, CD34, c-KIT, THY1) as shown.

Characterization of the cell lines established from EpCAM⁺ cells

As in freshly isolated EpCAM⁺ cells, CK19 and ALB were expressed in the established cell lines after 30 days of culture, as evidenced by RT-PCR and immunostaining (Fig. 6C,D). *Afp*, a marker of fetal liver progenitor cells, was expressed in the cultured cells (Fig. 6C), whereas it was not expressed in freshly isolated mouse oval cells, suggesting that more immature cells might be selected from EpCAM⁺ cells of NPCs in DDC liver. Alternatively, these proliferating cells might acquire a more hepatoblast-like character when cultured in vitro as previously reported (Schmelzer et al., 2007). In accordance with the latter idea, *Epcam* expression gradually decreased in culture (Fig. 6C). At the onset of mouse liver development, EpCAM is highly expressed in delta-like 1 homolog (DLK1)-positive hepatoblasts; however, its expression in hepatoblasts is dramatically reduced as liver development proceeds (our unpublished data). The reduction of EpCAM expression in cultured cells observed in this study is in line with the possibility that EpCAM⁺ cells might shift from an HSC-character to a more hepatoblast-like character.

To investigate the bipotency of cultured hepatic stem-like cells derived from EpCAM⁺ cells (HSCEs) at the clonal level, we randomly picked several clones and finally established 12 independent cell lines (HSCE1-12). All the expanded clones expressed both hepatocytic (*Alb*) and cholangiocytic (*Ck7*, *Ck19*) genes (see Table S2 in the supplementary material). The expression of *c-Met*, which is known to be expressed in oval cells, was also detected in all clones. Whereas tyrosine aminotransferase (*Tat*), a marker of perinatal hepatocytes, was weakly expressed in some of the clones, glucose-6-phosphatase (*G6Pase*; *G6pc*), another marker of perinatal hepatocytes, and carbamoyl phosphate synthetase (*Cps*), an adult hepatocyte marker, were rarely expressed (2/12 and 0/12, respectively). *Afp*, an immature hepatocyte marker, was expressed in most of the clones (10/12). These results indicated that HSCEs maintain immature characteristics.

Differentiation of clonally expanded EpCAM⁺ cells into the hepatocytic lineage in vitro

To address whether the established clones can differentiate into hepatocytic and cholangiocytic lineages, we used two clones, HSCE1 and HSCE2, and examined their differentiation potential. To induce hepatocytic differentiation and maturation, we utilized an in vitro culture system reported previously (Kamiya et al., 1999; Kamiya et al., 2002). Oncostatin M (OSM) is a powerful inducer of the differentiation of fetal hepatocytes and the addition of Engelbreth-Holm-Swarm (EHS) gel enhances hepatocyte maturation. Dimethyl sulfoxide (DMSO) is also known to maintain the differentiation of hepatocytes in culture (Isom et al., 1985; Sakai et al., 2002). By combining these methods, the expression of metabolic enzymes and transporters was monitored in two clones (Fig. 7A). Because both clones exhibited a similar profile, only the results of HSEC1 are shown. The expression of *G6Pase*, *Cps*, *Tat*, tryptophan-2,3-dioxygenase (*Tdo2*) and solute carrier family 10 (sodium/bile acid cotransporter family), member 1 (*Slc10a1*) was markedly induced by the addition of OSM, DMSO and EHS gel (Fig. 7B). By contrast, the expression of *Ck19* and of *Afp*, a marker of immature fetal hepatocytes, was downregulated. In addition, the PAS reaction showed that there were many clusters of hepatocytic

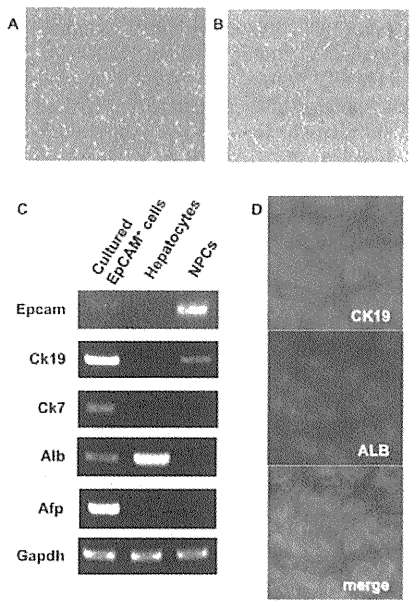

Fig. 6. EpCAM⁺ cells derived from DDC liver have high proliferative potential. (**A**,**B**) In vitro culture of EpCAM⁺ cells. Freshly isolated EpCAM⁺ cells from DDC liver were seeded on type-I collagen-coated dishes in the presence of HGF, EGF and IL6. The morphology of the cells after 5 days of culture (A) and after several passages (B) is shown. (**C**) RT-PCR of EpCAM⁺ cells after 30 days of culture. *Afp* was strongly expressed in the cultured cells. (**D**) Immunostaining of the cultured cells with anti-CK19 and anti-ALB antibodies.

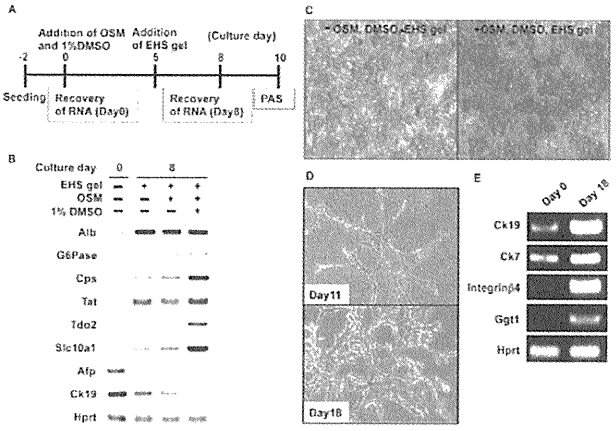

Fig. 7. Clonally expanded HSCEs can differentiate into both hepatocytes and cholangiocytes. (**A**) Experimental design for the differentiation of hepatic stem-like cells derived from EpCAM$^+$ cells (HSCEs) into hepatocytic cells. (**B**) RT-PCR of clone HSCE1 after hepatocytic differentiation. The addition of OSM, DMSO and EHS gel strongly induced the expression of hepatocytic genes and downregulated that of hepatoblastic and cholangiocytic genes. (**C**) PAS staining of HSCE1. The addition of OSM, DMSO and EHS gel strongly induced the accumulation of glycogen. (**D**) Morphological changes of HSCE1 after cholangiocytic differentiation. Tubules and branching morphology were clearly observed after 11 days of culture. (**E**) RT-PCR of HSCE1 after cholangiocytic differentiation. The expression of cholangiocytic marker genes was markedly upregulated in HSCE1.

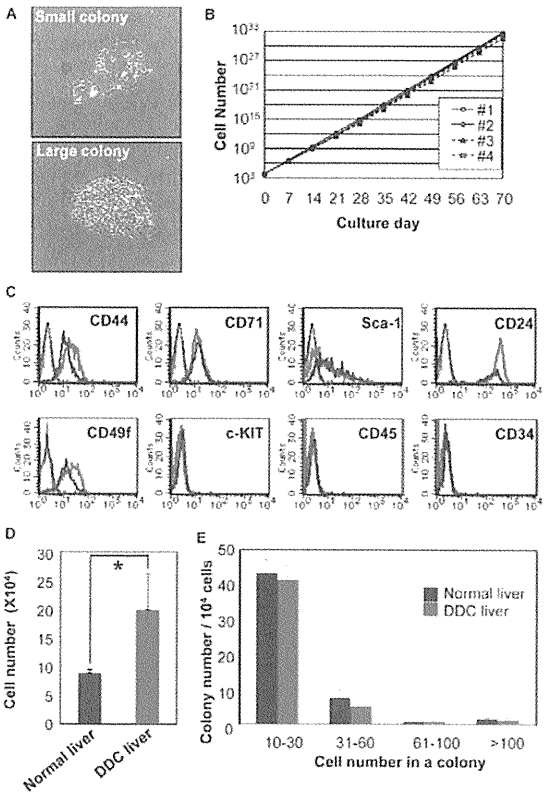

Fig. 8. Comparison between EpCAM$^+$ cells isolated from normal and injured liver. (**A**) Colony formation assay of EpCAM$^+$ cells from normal liver. Representative morphology of a small colony (top) and a large colony (bottom). Large colonies composed of more than 100 cells after 9 days of culture proliferate exponentially. (**B**) Unlimited cell proliferation of the established clones (#1-#4) in in vitro culture. (**C**) Comparison of cell surface markers between HSCEs from normal (blue line) and injured (red line) liver by FCM. Control IgG is in gray. The expression profiles of cell surface markers were similar in both HSCEs. (**D**) The number of EpCAM$^+$ cells per normal (n=4) or injured (n=6) liver. The number was estimated from the percentage of EpCAM$^+$ cells after immunomagnetic bead selection (see Fig. S2 in the supplementary material). There was a significant increase in EpCAM$^+$ cells in DDC liver (*P<0.01). (**E**) Colony formation assay of EpCAM$^+$ cells from normal and injured liver of mice fed DDC for 4 weeks. The data are derived from four independent experiments. Error bars, s.d.

cells accumulating glycogen (Fig. 7C). These results strongly suggested that clonally expanded HSCEs differentiate into the hepatocytic lineage.

Differentiation of clonally expanded EpCAM$^+$ cells into the cholangiocytic lineage in vitro

To evaluate the potential for differentiation into cholangiocytes, we utilized a three-dimensional collagen gel culture that is effective for the formation of tubules (Nishikawa et al., 1996; Tanimizu et al., 2004a). A cell suspension in collagen type-I gel was plated onto a basal layer of a collagen type-I gel and then culture medium containing HGF, an inducer of tubulogenesis, was loaded on top. After 11 days of culture, the formation of tubules was observed, and after 18 days of culture branching structures were clearly evident (Fig. 7D). In addition, RT-PCR revealed that the expression of cholangiocytic marker genes was upregulated in the cultured cells (Fig. 7E), indicating that HSCEs differentiated into the cholangiocytic lineage. Thus, EpCAM was expressed on oval cells in DDC liver and the clonally expanded cells from sorted EpCAM$^+$ cells exhibited characteristics of HSCs, i.e. unlimited proliferation and bi-directional differentiation. However, it remained unclear whether the emergence of such potential HSCs was an event restricted to liver injury and whether they were derived from oval cells.

EpCAM$^+$ cells in normal liver include potential HSCs

Because EpCAM$^+$ cells are present in normal mouse liver, we investigated whether potential HSCs are present among EpCAM$^+$ cells of normal liver. Interestingly, the colony formation assay revealed that sorted EpCAM$^+$ cells from normal liver formed both small and large colonies (Fig. 8A). These large colonies, which were composed of more than 100 cells, continued to proliferate, and these clones propagated continuously and exhibited bipotency similar to the HSCE clones derived from DDC liver (Fig. 8B and data not shown). In addition, HSCEs derived from normal and DDC liver exhibited a similar expression pattern of cell surface markers, strongly suggesting that they are closely related (Fig. 8C). By contrast, EpCAM$^-$ cells from normal or DDC liver did not give rise to any colonies, even when ten times more cells were plated than for EpCAM$^+$ (data not shown). If oval cells themselves have characteristics of potential HSCs then oval cell activation by the DDC diet should increase the number of potential HSCs. To test this possibility, we compared the number of EpCAM$^-$ cells and potential HSCs between normal and DDC liver (see Fig. S1 in the supplementary material). As shown in Fig. 8D, the number of

EpCAM$^+$ cells recovered from a DDC liver was approximately twice that from a normal liver. Interestingly, the numbers of large colonies corresponding to potential HSCs were very similar for normal and injured liver (Fig. 8E). In addition, adult potential HSCs are a very small population of EpCAM$^+$ cells in normal and injured liver. Although we cannot exclude the possibility that potential HSCs might increase slightly (not more than 2-fold), it is unlikely that the activation of oval cells by liver injury significantly increases the number of potential HSCs.

DISCUSSION

Oval cells have been considered adult liver stem/progenitor cells (Fausto, 2004; Oertel and Shafritz, 2008). However, previous studies were mostly histochemical, or involved biochemical and molecular biological characterization using cell fractions prepared by density gradient techniques. FCM is a powerful means of characterizing a particular type of cell, as successfully demonstrated by the identification of a very rare population of hematopoietic stem cells using a combination of cell surface markers (Osawa et al., 1996). In fetal liver, we and others reported the isolation and characterization of hepatoblasts by FCM using several markers (Kubota and Reid, 2000; Suzuki et al., 2002; Tanimizu et al., 2003). Although definitive proof of stemness requires a clonal analysis of freshly isolated oval cells, a lack of specific markers has hampered the precise identification and prospective isolation of oval cells from NPCs by FCM. To address this issue, we first searched for cell surface molecules expressed on oval cells and showed that anti-EpCAM antibody is useful for isolating oval cells from the liver of DDC-fed mice by cell sorting. Clonal analyses provide strong evidence that the EpCAM$^+$ cells from DDC liver contain adult potential HSCs that possess the capacity for unlimited proliferation and bi-directional differentiation.

Hepatic stem/progenitor cells have been considered to contribute to the regeneration of damaged liver when the proliferation of hepatocytes is restricted, and cell lines with HSC characteristics have been established from chemically damaged and/or genetically dysfunctional liver (Braun et al., 1987; Dumble et al., 2002; Sugiyama et al., 1997; Suzuki et al., 2008; Tirnitz-Parker et al., 2007; Yin et al., 1999). However, it remained unclear whether such cells are present in normal adult liver. Cell lines with HSC characteristics have been established from normal mouse (Fougere-Deschatrette et al., 2006), human (Herrera et al., 2006) and rat (Sahin et al., 2008) liver. However, these cell lines were derived from a hepatocyte-enriched cell population by centrifugation using a Percoll gradient or from unfractionated cells, leaving their origin ambiguous. Recently, Schmelzer et al. reported that EpCAM$^+$ cells from postnatal human donors include HSCs (Schmelzer et al., 2007). In this report, we demonstrate that EpCAM$^+$ cells isolated from normal or DDC mouse liver by FCM include potential HSCs. Interestingly, only a limited population of EpCAM$^+$ cells formed large colonies and the number of potential HSCs was not significantly increased in DDC liver compared with normal liver. Thus, our results strongly suggest that most mouse oval cells do not possess self-renewal potential and are likely to represent transit-amplifying cells that differentiate into mature hepatic cells.

Cholangiocytes proliferate under various pathological conditions. Cholangiocytes proliferate from pre-existing ducts in portal areas after PH or bile duct ligation in rats. Oval cell proliferation or ductular hyperplasia is induced by a number of chemicals, including 2-AAF, DDC (Preisegger et al., 1999) and by a choline-deficient ethionine-supplemented diet (Tian et al., 1997), and the proliferating cells form disorganized tubular structures that sprout into liver lobules. Selective damage of the periportal zone reduces such proliferation, supporting the notion that oval cells derive from the periportal region, in particular from the canals of Hering that connect the bile canaliculus and the biliary tree (Paku et al., 2001). However, the origin of oval cells is controversial and bone marrow stem cells were suggested to be a source (Petersen et al., 1999; Sell, 2001), although several reports refute this possibility (Menthena et al., 2004; Wang et al., 2003). Oval cells and cholangiocytes are not clearly distinguishable at the molecular level. In fact, oval cells and normal cholangiocytes are known to express many intracellular and membrane proteins in common, including EpCAM and CD133. However, it is also reported that some genes are predominantly expressed in rat or mouse oval cells. The expression of THY1, c-KIT and CD34 in oval cells has been controversial and these are also found in hematopoietic and mesenchymal cells (Dezso et al., 2007; Yovchev et al., 2008). By contrast, TROP2 is not expressed at all in normal liver and only in the oval cells of injured liver, indicating that TROP2 is a useful marker for oval cells.

Intriguingly, after oval cell activation, most of the EpCAM$^+$ cells express TROP2, and the original normal cholangiocytes, i.e. the EpCAM$^+$ TROP2$^-$ cells, are hardly detected by FCM and immunostaining. These results raise the possibility that not only oval cells but also activated cholangiocytes might begin to express TROP2 after liver injury and partly contribute to oval cell proliferation in this mouse model (Fig. 9). Alternatively, oval cells that are activated to proliferate during DDC administration and that express both EpCAM and TROP2 might continue to express both of these markers at least transiently after they differentiate into mature cholangiocytes. Further investigation into the expression profile of TROP2 in cholangiocytes would provide a clue as to the origin of oval cells. Moreover, the function of EpCAM and TROP2 in oval cell activation is an interesting issue that remains to be addressed.

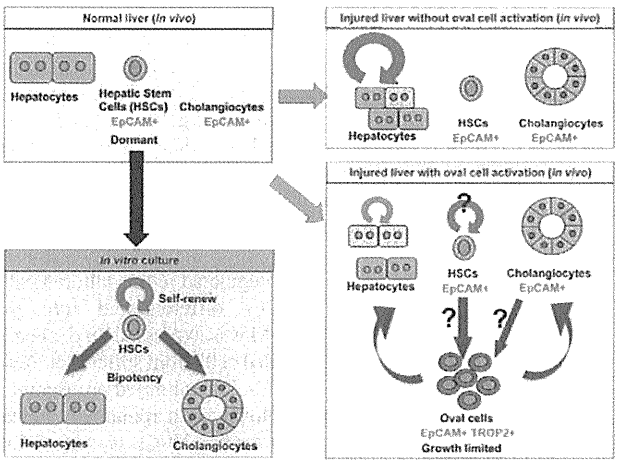

Fig. 9. Model of the hepatic stem/progenitor cell system in vivo and in vitro. Potential HSCs exist in normal liver as EpCAM$^+$ cells. They can proliferate unlimitedly and differentiate into both hepatocytes and cholangiocytes in vitro. Upon liver injury without oval cell activation, hepatocytes proliferate and contribute to liver regeneration. Upon liver injury with oval cell activation, EpCAM$^+$ TROP2$^+$ cells appear around portal veins to regenerate the liver. The oval cells might be partly derived from EpCAM$^+$ cholangiocytes. Most oval cells lacked the potential to self-renew in the in vitro colony formation assay.

Oval cells are believed to be involved in the regeneration of liver following injury. In addition, they are also considered as a cellular precursor for hepatocellular carcinoma (HCC) (Knight et al., 2005). Most of the experimental procedures used to induce oval cell proliferation in the liver ultimately lead to tumorigenesis. However, the connection between oval cells and tumorigenesis remains unclear. EpCAM is expressed on many normal as well as neoplastic epithelial cells and tumor-initiating cells (Al-Hajj et al., 2003; Armstrong and Eck, 2003; Momburg et al., 1987). Most recently, Maetzel et al. reported that EpCAM is a potent signal transducer and that its cleaved intracellular domain utilizes components of the Wnt pathway to induce cell proliferation (Maetzel et al., 2009). Such signaling via EpCAM might be involved in oval cell proliferation. Conversely, *Epcam* is itself a Wnt/β-catenin signaling target gene in HCC cell lines (Yamashita et al., 2007). Consistently, the involvement of the Wnt/β-catenin pathway in the oval cell response has been reported (Apte et al., 2008; Hu et al., 2007; Yang et al., 2008). We recently reported that *Wnt7a*, *Wnt7b* and *Wnt10a* are upregulated in DDC liver and that the Wnt/β-catenin pathway is likely to be involved in oval cell activation in vivo (Itoh et al., 2009). Therefore, the correlation between tumorigenesis and the expression of EpCAM in oval cells is plausible. Because EpCAM is widely expressed in normal epithelial cells, including biliary epithelial cells, the expression and signaling of EpCAM should be tightly regulated at the steady state. However, the regulation of EpCAM signaling in normal and malignant stem-like cells remains unknown.

It is also reported that TROP2 is expressed on cells of some normal tissues as well as on cancer cells (El Sewedy et al., 1998; Huang et al., 2005; Ohmachi et al., 2006). Our finding that TROP2, a member of the EpCAM family, is upregulated in oval cells raises the possibility that TROP2 might modulate and/or enhance the intracellular signaling of EpCAM to promote proliferation and migration into liver parenchyma. Alternatively, TROP2 itself might transduce intracellular signaling in a manner similar to EpCAM. In fact, ectopic expression of TROP2 in NIH3T3 cells is sufficient to promote both anchorage-independent growth and tumorigenesis (Wang et al., 2008). Most recently, Goldstein et al. reported that TROP2 identifies a subpopulation of murine and human prostate basal cells with stem cell characteristics (Goldstein et al., 2008), suggesting an association between TROP2 and stem/progenitor cells.

Although chronic liver injury induces the proliferation of oval cells in some rodent models and in human disease, the underlying relationship between oval cells and HSCs and their developmental mechanisms require further investigation. We showed the presence of potential HSCs in normal liver, as well as in injured liver, by isolating $EpCAM^+$ cells and demonstrated the expression of TROP2 in oval cells. Further investigation into the interaction between EpCAM and TROP2 in oval cells will help us to understand the mechanisms of growth and differentiation in cancer-initiating cells as well as in normal stem/progenitor cells.

Anti-A6 antibody was kindly provided by Dr Snorri Thorgeirsson and Dr Valentina Factor. This work was supported in part by a grant for Core Research for Evolutionary Science and Technology from the Japan Science and Technology Agency (JST) and a research grant from the Ministry of Education, Sports, Science and Technology (Japan).

Supplementary material

Supplementary material available online at
http://dev.biologists.org/cgi/content/full/136/11/1951/DC1

References

Akhurst, B., Croager, E. J., Farley-Roche, C. A., Ong, J. K., Dumble, M. L., Knight, B. and Yeoh, G. C. (2001). A modified choline-deficient, ethionine-supplemented diet protocol effectively induces oval cells in mouse liver. *Hepatology* **34**, 519-522.

Al-Hajj, M., Wicha, M. S., Benito-Hernandez, A., Morrison, S. J. and Clarke, M. F. (2003). Prospective identification of tumorigenic breast cancer cells. *Proc. Natl. Acad. Sci. USA* **100**, 3983-3988.

Alison, M. R., Golding, M., Sarraf, C. E., Edwards, R. J. and Lalani, E. N. (1996). Liver damage in the rat induces hepatocyte stem cells from biliary epithelial cells. *Gastroenterology* **110**, 1182-1190.

Apte, U., Thompson, M. D., Cui, S., Liu, B., Cieply, B. and Monga, S. P. (2008). Wnt/beta-catenin signaling mediates oval cell response in rodents. *Hepatology* **47**, 288-295.

Armstrong, A. and Eck, S. L. (2003). EpCAM: A new therapeutic target for an old cancer antigen. *Cancer Biol. Ther.* **2**, 320-326.

Braun, L., Goyette, M., Yaswen, P., Thompson, N. L. and Fausto, N. (1987). Growth in culture and tumorigenicity after transfection with the ras oncogene of liver epithelial cells from carcinogen-treated rats. *Cancer Res.* **47**, 4116-4124.

de Boer, C. J., van Krieken, J. H., Janssen-van Rhijn, C. M. and Litvinov, S. V. (1999). Expression of Ep-CAM in normal, regenerating, metaplastic, and neoplastic liver. *J. Pathol.* **188**, 201-206.

Dezso, K., Jelnes, P., Laszlo, V., Baghy, K., Bodor, C., Paku, S., Tygstrup, N., Bisgaard, H. C. and Nagy, P. (2007). Thy-1 is expressed in hepatic myofibroblasts and not oval cells in stem cell-mediated liver regeneration. *Am. J. Pathol.* **171**, 1529-1537.

Dumble, M. L., Croager, E. J., Yeoh, G. C. and Quail, E. A. (2002). Generation and characterization of p53 null transformed hepatic progenitor cells: oval cells give rise to hepatocellular carcinoma. *Carcinogenesis* **23**, 435-445.

El Sewedy, T., Fornaro, M. and Alberti, S. (1998). Cloning of the murine TROP2 gene: conservation of a PIP2-binding sequence in the cytoplasmic domain of TROP-2. *Int. J. Cancer* **75**, 324-330.

Engelhardt, N. V., Factor, V. M., Medvinsky, A. L., Baranov, V. N., Lazareva, M. N. and Poltoranina, V. S. (1993). Common antigen of oval and biliary epithelial cells (A6) is a differentiation marker of epithelial and erythroid cell lineages in early development of the mouse. *Differentiation* **55**, 19-26.

Evarts, R. P., Nagy, P., Marsden, E. and Thorgeirsson, S. S. (1987). A precursor-product relationship exists between oval cells and hepatocytes in rat liver. *Carcinogenesis* **8**, 1737-1740.

Farber, E. (1956). Similarities in the sequence of early histological changes induced in the liver of the rat by ethionine, 2-acetylamino-fluorene, and 3'-methyl-4-dimethylaminoazobenzene. *Cancer Res.* **16**, 142-148.

Fausto, N. (2004). Liver regeneration and repair: hepatocytes, progenitor cells, and stem cells. *Hepatology* **39**, 1477-1487.

Fonia, O., Weizman, R., Coleman, R., Kaganovskaya, E. and Gavish, M. (1996). PK 11195 aggravates 3,5-diethoxycarbonyl-1,4-dihydrocollidine-induced hepatic porphyria in rats. *Hepatology* **24**, 697-701.

Fougere-Deschatrette, C., Imaizumi-Scherrer, T., Strick-Marchand, H., Morosan, S., Charneau, P., Kremsdorf, D., Faust, D. M. and Weiss, M. C. (2006). Plasticity of hepatic cell differentiation: bipotential adult mouse liver clonal cell lines competent to differentiate in vitro and in vivo. *Stem Cells* **24**, 2098-2109.

Gleiberman, A. S., Encinas, J. M., Mignone, J. L., Michurina, T., Rosenfeld, M. G. and Enikolopov, G. (2005). Expression of nestin-green fluorescent protein transgene marks oval cells in the adult liver. *Dev. Dyn.* **234**, 413-421.

Goldstein, A. S., Lawson, D. A., Cheng, D., Sun, W., Garraway, I. P. and Witte, O. N. (2008). Trop2 identifies a subpopulation of murine and human prostate basal cells with stem cell characteristics. *Proc. Natl. Acad. Sci. USA* **105**, 20882-20887.

Hara, T., Nakano, Y., Tanaka, M., Tamura, K., Sekiguchi, T., Minehata, K., Copeland, N. G., Jenkins, N. A., Okabe, M., Kogo, H. et al. (1999). Identification of podocalyxin-like protein 1 as a novel cell surface marker for hemangioblasts in the murine aorta-gonad-mesonephros region. *Immunity* **11**, 567-578.

Herrera, M. B., Bruno, S., Buttiglieri, S., Tetta, C., Gatti, S., Deregibus, M. C., Bussolati, B. and Camussi, G. (2006). Isolation and characterization of a stem cell population from adult human liver. *Stem Cells* **24**, 2840-2850.

Hreha, G., Jefferson, D. M., Yu, C. H., Grubman, S. A., Alsabeh, R., Geller, S. A. and Vierling, J. M. (1999). Immortalized intrahepatic mouse biliary epithelial cells: immunologic characterization and immunogenicity. *Hepatology* **30**, 358-371.

Hu, M., Kurobe, M., Jeong, Y. J., Fuerer, C., Ghole, S., Nusse, R. and Sylvester, K. G. (2007). Wnt/beta-catenin signaling in murine hepatic transit amplifying progenitor cells. *Gastroenterology* **133**, 1579-1591.

Huang, H., Groth, J., Sossey-Alaoui, K., Hawthorn, L., Beall, S. and Geradts, J. (2005). Aberrant expression of novel and previously described cell membrane markers in human breast cancer cell lines and tumors. *Clin. Cancer Res.* **11**, 4357-4364.

Isom, H. C., Secott, T., Georgoff, I., Woodworth, C. and Mummaw, J. (1985). Maintenance of differentiated rat hepatocytes in primary culture. *Proc. Natl. Acad. Sci. USA* **82**, 3252-3256.

Itoh, T., Kamiya, Y., Okabe, M., Tanaka, M. and Miyajima, A. (2009). Inducible expression of Wnt genes during adult hepatic stem/progenitor cell response. *FEBS Lett.* **583**, 777-781.
Jelnes, P., Santoni-Rugiu, E., Rasmussen, M., Friis, S. L., Nielsen, J. H., Tygstrup, N. and Bisgaard, H. C. (2007). Remarkable heterogeneity displayed by oval cells in rat and mouse models of stem cell-mediated liver regeneration. *Hepatology* **45**, 1462-1470.
Joplin, R., Strain, A. J. and Neuberger, J. M. (1990). Biliary epithelial cells from the liver of patients with primary biliary cirrhosis: isolation, characterization, and short-term culture. *J. Pathol.* **162**, 255-260.
Kamiya, A., Kinoshita, T., Ito, Y., Matsui, T., Morikawa, Y., Senba, E., Nakashima, K., Taga, T., Yoshida, K., Kishimoto, T. et al. (1999). Fetal liver development requires a paracrine action of oncostatin M through the gp130 signal transducer. *EMBO J.* **18**, 2127-2136.
Kamiya, A., Kojima, N., Kinoshita, T., Sakai, Y. and Miyaijma, A. (2002). Maturation of fetal hepatocytes in vitro by extracellular matrices and oncostatin M: induction of tryptophan oxygenase. *Hepatology* **35**, 1351-1359.
Knight, B., Matthews, V. B., Olynyk, J. K. and Yeoh, G. C. (2005). Jekyll and Hyde: evolving perspectives on the function and potential of the adult liver progenitor (oval) cell. *BioEssays* **27**, 1192-1202.
Kojima, T. and Kitamura, T. (1999). A signal sequence trap based on a constitutively active cytokine receptor. *Nat. Biotechnol.* **17**, 487-490.
Kubota, H. and Reid, L. M. (2000). Clonogenic hepatoblasts, common precursors for hepatocytic and biliary lineages, are lacking classical major histocompatibility complex class I antigen. *Proc. Natl. Acad. Sci. USA* **97**, 12132-12137.
Laishes, B. A. and Rolfe, P. B. (1981). Search for endogenous liver colony-forming units in F344 rats given a two-thirds hepatectomy during short-term feeding of 2-acetylaminofluorene. *Cancer Res.* **41**, 1731-1741.
Lee, J. S., Heo, J., Libbrecht, L., Chu, I. S., Kaposi-Novak, P., Calvisi, D. F., Mikaelyan, A., Roberts, L. R., Demetris, A. J., Sun, Z. et al. (2006). A novel prognostic subtype of human hepatocellular carcinoma derived from hepatic progenitor cells. *Nat. Med.* **12**, 410-416.
Lemaigre, F. P. (2003). Development of the biliary tract. *Mech. Dev.* **120**, 81-87.
Maetzel, D., Denzel, S., Mack, B., Canis, M., Went, P., Benk, M., Kieu, C., Papior, P., Baeuerle, P. A., Munz, M. et al. (2009). Nuclear signalling by tumour-associated antigen EpCAM. *Nat. Cell Biol.* **11**, 162-171.
Menthena, A., Deb, N., Oertel, M., Grozdanov, P. N., Sandhu, J., Shah, S., Guha, C., Shafritz, D. A. and Dabeva, M. D. (2004). Bone marrow progenitors are not the source of expanding oval cells in injured liver. *Stem Cells* **22**, 1049-1061.
Michalopoulos, G. K. and DeFrances, M. C. (1997). Liver regeneration. *Science* **276**, 60-66.
Momburg, F., Moldenhauer, G., Hammerling, G. J. and Moller, P. (1987). Immunohistochemical study of the expression of a Mr 34,000 human epithelium-specific surface glycoprotein in normal and malignant tissues. *Cancer Res.* **47**, 2883-2891.
Nishikawa, Y., Tokusashi, Y., Kadohama, T., Nishimori, H. and Ogawa, K. (1996). Hepatocytic cells form bile duct-like structures within a three-dimensional collagen gel matrix. *Exp. Cell Res.* **223**, 357-371.
Notenboom, R. G., van den Bergh Weerman, M. A., Dingemans, K. P., Vermeulen, J. L., van den Eijnde, S., Reutelingsperger, C. P., Hut, H., Willemsen, R., Offerhaus, G. J. and Lamers, W. H. (2003). Timing and sequence of differentiation of embryonic rat hepatocytes along the biliary epithelial lineage. *Hepatology* **38**, 683-691.
Oertel, M. and Shafritz, D. A. (2008). Stem cells, cell transplantation and liver repopulation. *Biochim. Biophys. Acta* **1782**, 61-74.
Ohmachi, T., Tanaka, F., Mimori, K., Inoue, H., Yanaga, K. and Mori, M. (2006). Clinical significance of TROP2 expression in colorectal cancer. *Clin. Cancer Res.* **12**, 3057-3063.
Osawa, M., Hanada, K., Hamada, H. and Nakauchi, H. (1996). Long-term lymphohematopoietic reconstitution by a single CD34-low/negative hematopoietic stem cell. *Science* **273**, 242-245.
Overturf, K., al-Dhalimy, M., Ou, C. N., Finegold, M. and Grompe, M. (1997). Serial transplantation reveals the stem-cell-like regenerative potential of adult mouse hepatocytes. *Am. J. Pathol.* **151**, 1273-1280.
Paku, S., Schnur, J., Nagy, P. and Thorgeirsson, S. S. (2001). Origin and structural evolution of the early proliferating oval cells in rat liver. *Am. J. Pathol.* **158**, 1313-1323.
Petersen, B. E., Goff, J. P., Greenberger, J. S. and Michalopoulos, G. K. (1998). Hepatic oval cells express the hematopoietic stem cell marker Thy-1 in the rat. *Hepatology* **27**, 433-445.
Petersen, B. E., Bowen, W. C., Patrene, K. D., Mars, W. M., Sullivan, A. K., Murase, N., Boggs, S. S., Greenberger, J. S. and Goff, J. P. (1999). Bone marrow as a potential source of hepatic oval cells. *Science* **284**, 1168-1170.
Preisegger, K. H., Factor, V. M., Fuchsbichler, A., Stumptner, C., Denk, H. and Thorgeirsson, S. S. (1999). Atypical ductular proliferation and its inhibition by transforming growth factor beta1 in the 3,5-diethoxycarbonyl-1,4-dihydrocollidine mouse model for chronic alcoholic liver disease. *Lab. Invest.* **79**, 103-109.
Roskams, T. A., Theise, N. D., Balabaud, C., Bhagat, G., Bhathal, P. S., Bioulac-Sage, P., Brunt, E. M., Crawford, J. M., Crosby, H. A., Desmet, V. et al. (2004). Nomenclature of the finer branches of the biliary tree: canals, ductules, and ductular reactions in human livers. *Hepatology* **39**, 1739-1745.
Rountree, C. B., Barsky, L., Ge, S., Zhu, J., Senadheera, S. and Crooks, G. M. (2007). A CD133-expressing murine liver oval cell population with bilineage potential. *Stem Cells* **25**, 2419-2429.
Sahin, M. B., Schwartz, R. E., Buckley, S. M., Heremans, Y., Chase, L., Hu, W. S. and Verfaillie, C. M. (2008). Isolation and characterization of a novel population of progenitor cells from unmanipulated rat liver. *Liver Transpl.* **14**, 333-345.
Sakai, Y., Jiang, J., Kojima, N., Kinoshita, T. and Miyajima, A. (2002). Enhanced in vitro maturation of fetal mouse liver cells with oncostatin M, nicotinamide, and dimethyl sulfoxide. *Cell Transplant.* **11**, 435-441.
Schmelzer, E., Zhang, L., Bruce, A., Wauthier, E., Ludlow, J., Yao, H. L., Moss, N., Melhem, A., McClelland, R., Turner, W. et al. (2007). Human hepatic stem cells from fetal and postnatal donors. *J. Exp. Med.* **204**, 1973-1987.
Seglen, P. O. (1976). Preparation of isolated rat liver cells. *Methods Cell Biol.* **13**, 29-83.
Sell, S. (2001). Heterogeneity and plasticity of hepatocyte lineage cells. *Hepatology* **33**, 738-750.
Sugiyama, K., Kato, N., Mizutani, T., Ikeda, M., Tanaka, T. and Shimotohno, K. (1997). Genetic analysis of the hepatitis C virus (HCV) genome from HCV-infected human T cells. *J. Gen. Virol.* **78**, 329-336.
Suzuki, A., Zheng, Y. W., Kaneko, S., Onodera, M., Fukao, K., Nakauchi, H. and Taniguchi, H. (2002). Clonal identification and characterization of self-renewing pluripotent stem cells in the developing liver. *J. Cell Biol.* **156**, 173-184.
Suzuki, A., Sekiya, S., Onishi, M., Oshima, N., Kiyonari, H., Nakauchi, H. and Taniguchi, H. (2008). Flow cytometric isolation and clonal identification of self-renewing bipotent hepatic progenitor cells in adult mouse liver. *Hepatology* **48**, 1964-1978.
Tanimizu, N., Nishikawa, M., Saito, H., Tsujimura, T. and Miyajima, A. (2003). Isolation of hepatoblasts based on the expression of Dlk/Pref-1. *J. Cell Sci.* **116**, 1775-1786.
Tanimizu, N., Saito, H., Mostov, K. and Miyajima, A. (2004a). Long-term culture of hepatic progenitors derived from mouse Dlk+ hepatoblasts. *J. Cell Sci.* **117**, 6425-6434.
Tanimizu, N., Tsujimura, T., Takahide, K., Kodama, T., Nakamura, K. and Miyajima, A. (2004b). Expression of Dlk/Pref-1 defines a subpopulation in the oval cell compartment of rat liver. *Gene Expr. Patterns* **5**, 209-218.
Theise, N. D., Saxena, R., Portmann, B. C., Thung, S. N., Yee, H., Chiriboga, L., Kumar, A. and Crawford, J. M. (1999). The canals of Hering and hepatic stem cells in humans. *Hepatology* **30**, 1425-1433.
Tian, Y. W., Smith, P. G. and Yeoh, G. C. (1997). The oval-shaped cell as a candidate for a liver stem cell in embryonic, neonatal and precancerous liver: identification based on morphology and immunohistochemical staining for albumin and pyruvate kinase isoenzyme expression. *Histochem. Cell Biol.* **107**, 243-250.
Tirnitz-Parker, J. E., Tonkin, J. N., Knight, B., Olynyk, J. K. and Yeoh, G. C. (2007). Isolation, culture and immortalisation of hepatic oval cells from adult mice fed a choline-deficient, ethionine-supplemented diet. *Int. J. Biochem. Cell Biol.* **39**, 2226-2239.
Wang, J., Day, R., Dong, Y., Weintraub, S. J. and Michel, L. (2008). Identification of Trop-2 as an oncogene and an attractive therapeutic target in colon cancers. *Mol. Cancer Ther.* **7**, 280-285.
Wang, X., Foster, M., Al-Dhalimy, M., Lagasse, E., Finegold, M. and Grompe, M. (2003). The origin and liver repopulating capacity of murine oval cells. *Proc. Natl. Acad. Sci. USA* **100** (Suppl. 1), 11881-11888.
Watanabe, N., Tanaka, M., Suzuki, K., Kumanogoh, A., Kikutani, H. and Miyajima, A. (2007). Tim2 is expressed in mouse fetal hepatocytes and regulates their differentiation. *Hepatology* **45**, 1240-1249.
Went, P. T., Lugli, A., Meier, S., Bundi, M., Mirlacher, M., Sauter, G. and Dirnhofer, S. (2004). Frequent EpCam protein expression in human carcinomas. *Hum. Pathol.* **35**, 122-128.
Yamashita, T., Budhu, A., Forgues, M. and Wang, X. W. (2007). Activation of hepatic stem cell marker EpCAM by Wnt-beta-catenin signaling in hepatocellular carcinoma. *Cancer Res.* **67**, 10831-10839.
Yang, W., Yan, H. X., Chen, L., Liu, Q., He, Y. Q., Yu, L. X., Zhang, S. H., Huang, D. D., Tang, L., Kong, X. N. et al. (2008). Wnt/beta-catenin signaling contributes to activation of normal and tumorigenic liver progenitor cells. *Cancer Res.* **68**, 4287-4295.
Yin, L., Lynch, D. and Sell, S. (1999). Participation of different cell types in the restitutive response of the rat liver to periportal injury induced by allyl alcohol. *J. Hepatol.* **31**, 497-507.
Yovchev, M. I., Grozdanov, P. N., Joseph, B., Gupta, S. and Dabeva, M. D. (2007). Novel hepatic progenitor cell surface markers in the adult rat liver. *Hepatology* **45**, 139-149.
Yovchev, M. I., Grozdanov, P. N., Zhou, H., Racherla, H., Guha, C. and Dabeva, M. D. (2008). Identification of adult hepatic progenitor cells capable of repopulating injured rat liver. *Hepatology* **47**, 636-647.
Zaret, K. S. (2000). Liver specification and early morphogenesis. *Mech. Dev.* **92**, 83-88.

Molecular Biology of the Cell
Vol. 20, 2486–2494, May 1, 2009

Liver Progenitor Cells Fold Up a Cell Monolayer into a Double-layered Structure during Tubular Morphogenesis

Naoki Tanimizu,*† Atsushi Miyajima,† and Keith E. Mostov*

*Departments of Anatomy, and Biochemistry and Biophysics, University of California San Francisco, San Francisco, CA 94143-2140; and †Institute of Molecular and Cellular Biosciences, The University of Tokyo, Tokyo 113-0032, Japan

Submitted February 19, 2008; Revised February 27, 2009; Accepted March 3, 2009
Monitoring Editor: Asma Nusrat

Bile ducts are hepatic tubular structures that are lined by cholangiocytes, a type of liver epithelial cell. Cholangiocytes first form a single layer of cells, termed the ductal plate, surrounding the portal vein, which eventually remodels into the branching tubular network of bile ducts. The process of bile duct morphogenesis is not yet clear: a conventional model where cholangiocytes proliferate to duplicate a single layer of the ductal plate before lumen formation seems inconsistent with the observation that proliferation is dramatically reduced when hepatoblasts, liver progenitor cells, differentiate into cholangiocytes. Here, we developed a new culture system in which a liver progenitor cell line, HPPL, reorganizes from a monolayer to tubular structures in response to being overlaid with a gel containing type I collagen and Matrigel. We found that some of the HPPL in the monolayer depolarized and migrated to fold up the monolayer into a double-cell layer. These morphogenetic processes occurred without cell proliferation and required phosphatidylinositol 3-kinase and Akt activity. Later in morphogenesis, luminal space was generated between the two cell layers. This process, in particular enlargement of the apical lumen, involved transcriptional activity of HNF1β. Thus, using this sandwich culture system, we could segregate tubulogenesis of bile ducts into distinct steps and found that the PI3K/Akt pathway and HNF1β regulated different steps of the morphogenesis. Although the process of tubulogenesis in culture specifically resembled early bile duct formation, involvement of these two key players suggests that the sandwich culture might help us to find common principles of tubulogenesis in general.

INTRODUCTION

Tubules are an essential structural unit for numerous epithelial organs, such as lung, liver, and kidney. Epithelial tubes in different organs form by a wide variety of mechanisms (Hogan and Kolodziej, 2002; Lubarsky and Krasnow, 2003; Bryant and Mostov, 2008). Understanding the cellular and molecular basis of these mechanisms and discovering common principles that may underlie these diverse mechanisms is an important goal.

In the liver, bile ducts are tubular structures that consist of cholangiocytes, a type of liver epithelial cell. Bile ducts provide the excretory route for bile, which is synthesized by hepatocytes, another type of liver epithelial cell. Because bile is cytotoxic, abnormal development of bile ducts, which causes the accumulation of bile inside the liver, induces hepatic injury and ultimately results in severe liver fibrosis and cirrhosis (Schmucker *et al.*, 1990; Yoon and Gores, 2002; Paumgartner, 2006).

Cholangiocytes, the epithelial component of bile ducts, differentiate from liver progenitor cells called hepatoblasts around embryonic day 15 (E15) in mice (Lemaigre, 2003). Recent reports have identified the Notch and TGFβ signaling pathways and a transcription factor Hex, which regulate differentiation of cholangiocytes from hepatoblasts (McCright *et al.*, 2002; Kodama *et al.*, 2004; Tanimizu and Miyajima, 2004; Clotman *et al.*, 2005; Hunter *et al.*, 2007). After being induced, cholangiocytes acquire secretory functions and regulate the flow rate of bile and alkalinize it by secreting water and bicarbonate ion, respectively (Fitz, 2002). In parallel to this functional differentiation, cholangiocytes undergo tubular morphogenesis and develop the tubular tree of bile ducts.

Tubular morphogenesis of bile ducts has been studied by examining the structure of developing liver by histochemical techniques (Tan *et al.*, 1995). Cholangiocytes form a single-cell layer called the ductal plate around the portal vein; this ductal plate is then duplicated. Next, luminal space is generated between the two cholangiocyte layers. Finally, the ductal plate along with the luminal space is reorganized into tubules (Crawford, 2002). Recently, studies using mutant mice have identified several molecules necessary for tubular morphogenesis of bile ducts. In mice lacking HES1 (Kodama *et al.*, 2004) or lacking HNF1β specifically in the liver (Coffinier *et al.*, 2002), cholangiocytes differentiated from hepatoblasts but could not form bile duct tubules. Furthermore, abnormal formation of bile ducts that is generally recognized as "ductal plate malformation" has been reported in congenital human diseases such as Calori's disease and Meckel-Gruber syndrome (Low *et al.*, 2001). However, the precise mechanisms governing tubular morphogenesis of cholangiocytes have not been reported yet.

A major limitation in analyzing the mechanisms of intrahepatic bile duct formation has been a paucity of good cell culture models that recapitulate this process. To address these questions, we established an organotypic culture sys-

This article was published online ahead of print in *MBC in Press* (http://www.molbiolcell.org/cgi/doi/10.1091/mbc.E08-02-0177) on March 18, 2009.

Address correspondence to: Keith E. Mostov (keith.mostov@ucsf.edu).

tem in which liver progenitor cells form tubular structures. Considering that cholangiocytes make a single-cell layer of the ductal plate before tubular morphogenesis in vivo, we used a "sandwich" culture system. In this culture system, we cultured HPPL, a liver progenitor cell line, on the top of extracellular matrix (ECM) gel until they formed a monolayer and then placed another layer of gel over the monolayer. The top layer of gel induced the rearrangement of the monolayer into a double-cell layer and the generation of luminal space between the two cell layers. This novel culture system resembles development in vivo and has enabled us to address the mechanisms governing formation of bile duct tubules.

MATERIALS AND METHODS

Extracellular Matrix, Growth Factors, and Chemicals

Type I collagen was purchased from Cohesion Technologies (Palo Alto, CA). Growth factor reduced Matrigel and purified laminin-1 were from BD Biosciences (Bedford, MA). Mitomycin C (MMC) was from Sigma-Aldrich (St. Louis, MO). LY294002, a phosphatidylinositol 3-kinase (PI3K) inhibitor, and triciribine, an Akt inhibitor, were from Calbiochem (La Jolla, CA).

Cell Culture

HPPL were kept in DMEM/F12 (Sigma) containing 10% FBS (Invitrogen, Gaithersburg, MD), 1× insulin/transferrin/selenium (ITS; Invitrogen), 10 mM nicotinamide (Wako, Osaka, Japan), 0.1 μM dexamethasone (Dex; Sigma), 5 mM L-glutamine, 5 ng/ml hepatocyte growth factor (HGF; gift of the late Ralph Schwall, Genentech) and epidermal growth factor (EGF; Invitrogen, Carlsbad, CA). To prepare the bottom layer of culture, 1 volume of Matrigel were mixed with 4 volumes of type I collagen and 150 μl of the gel were added to each 1-cm diameter tissue culture insert (0.02-μm Anopore Membrane; Millipore, Billerica, MA). HPPL were plated on the bottom layer at a density of 1×10^5 cells. After 2 d of incubation, the monolayer of HPPL was overlaid with another layer of ECM gel. After incubation at 37°C for 2 h to solidify the gel, 500 μl of DMEM/F12 containing EGF and HGF were added to the top of the gel and under the culture insert.

To block proliferation, HPPL were incubated in the presence of 0.5 or 1 μg/ml MMC for 6 h before the overlay. To inhibit the activity of PI3K or Akt, HPPL were overlaid with ECM gel and then incubated in the presence of 20 μM LY294002 or 2 μM triciribine.

Immunofluorescence Microscopy

Mouse embryonic and neonatal livers were embedded in OCT compound and frozen. These were used for preparation of thin sections by using a cryostat (Leica, St. Gallen, Switzerland). Sections were incubated in PBS containing 4% paraformaldehyde (PFA) at 4°C for 10 min. Samples of sandwich culture were treated with collagenase and fixed in PFA solution as previously reported (O'Brien *et al.*, 2006). Primary antibodies used in this study were rabbit anti-cytokeratin 19 (CK19; 1:2000; Tanimizu *et al.*, 2003), rat anti-ZO1 (1:2000; a gift from Dr. Bruce Stevenson, University of Alberta), rat anti-Ki67 (1:200; Dako, Carpinteria, CA), rat anti-EpCAM (1:500; BD Biosciences), rabbit anti-Akt (1:100; Cell Signaling Technology, Danvers, MA), and rabbit anti-phospho-Thr308 Akt (1:100; Cell Signaling Technology) antibodies. Signals were visualized with AlexaFluor conjugated secondary antibodies (Molecular Probes, Eugene, OR) used at a dilution of 1:500. F-actin bundles were detected with AlexaFluor 488– or 546–conjugated phalloidin (Molecular Probes) at a dilution of 1:250. Nuclei were counterstained with Hoechst 34580. Samples were examined on Zeiss LSM 510 and Olympus FV1000D IX81 confocal laser scanning fluorescence microscopes (Thornwood and Melville, NY, respectively).

Overexpression of a Dominant Negative Form of HNF1β

The sequences of HNF1β263fsinGG (dominant negative HNF1β: dnHNF1β) were amplified from the first-strand cDNA derived from HPPL by using following primers: 5′-GCC ACC ATG GTG TCC AAG CTC ACG TCG C-3′ and 5′-GCG GCC GCC TAA CCG GCC TCC CTC TCT TCC TTG-3′. PCR products were inserted into pCRII vector (Invitrogen). After verifying the sequence, the fragment of dnHNF1β was transferred into EcoRI-NotI sites of pMXs-IRES-GFP. pMXs-dnHNF1β-IRES-GFP was introduced into BOSC23, a virus-packaging cell. Packaged virus collected from 10 ml of culture medium by centrifugation was resuspended in 2 ml of fresh medium. After incubating HPPL with virus solution for 2 d, infection efficiency was checked on a FACScalibur (BD Biosciences, San Diego, CA) by examining expression of green fluorescent protein (GFP).

Live Cell Imaging

HPPL expressing GFP were generated as described above. For imaging under a microscope, we used 24-well glass bottom dishes instead of culture inserts in order to permit focusing on cells in the culture. We selected four areas in a well and took ~16 X-Y images at different planes along the Z-axis using Olympus FV1000D IX81 confocal microscope. At 2 h after the overlay, we started taking images every 40 min for 24 h. Our system includes an Olympus ZDC system that ensures the constant distance between an objective lens and the bottom of the dish during imaging.

RESULTS

HPPL Form a Tubular Network in Sandwich Culture

Histochemical data indicate that cholangiocytes, which differentiate from hepatoblasts around the portal vein, form the single-cell layer of the ductal plate before starting tubular morphogenesis. The ductal plate is reorganized into bile duct tubules later in perinatal liver (Crawford, 2002). To mimic a process of tubular morphogenesis that starts from a single layer of cells, we overlaid ECM gel on top of a monolayer of liver progenitor cells. A similar protocol has been used with Madin-Darby canine kidney (MDCK) cells to induce tubular structures: MDCK cells generate a tubular network from a monolayer after overlaying with collagen gel (Hall *et al.*, 1982; Ojakian and Schwimmer, 1994; Zuk and Matlin, 1996; Ojakian *et al.*, 2001). For optimizing culture condition, we used HPPL, a liver progenitor cell line that differentiates into both hepatocytes and cholangiocytes in vitro (Tanimizu *et al.*, 2004). We first cultured HPPL on a culture insert coated with laminin until they formed a confluent monolayer, and then we covered the monolayer with either type I collagen gel or a mixture of type I collagen gel and Matrigel. However, HPPL did not form tubular structures under either condition. We then cultured HPPL on an ECM gel that was pure type I collagen gel, collagen gel containing 10, 20, 30, 40, or 60% Matrigel, or pure Matrigel. HPPL formed a monolayer on collagen gel containing 10 or 20% Matrigel. Therefore, we covered the monolayer on 20% Matrigel with a mixture of collagen and Matrigel that had the same composition as the bottom layer (Figure 1A). We called this system "sandwich culture."

Two days after the overlay, we visualized F-actin localization by incubating with AlexaFluor 488–conjugated phalloidin. We observed that HPPL formed areas surrounded by thick F-actin bundles (Figure 1B), suggesting that HPPL formed a tubular network where luminal space was surrounded by polarized cells. To better visualize the luminal space, we reconstructed images of confocal vertical (X-Z) sections after staining with anti-cytokeratin 19 (CK19), a cholangiocyte marker, F-actin, and ZO1 showing that HPPL expressed CK19 and localized ZO1 at the apical tip of the lateral domain surrounding the apical luminal space (Figure 1C). Thus, we considered that HPPL reorganized a monolayer into tubular structures in sandwich cultures.

Proliferation Is Not Necessary for Tubular Morphogenesis In Vitro

To test whether proliferation of HPPL is necessary for tubular morphogenesis, we blocked proliferation of HPPL by adding MMC, a DNA synthesis inhibitor, to the culture 6 h before the overlay. At 2 d after overlay, we estimated the area of the tubular structures by using NIH ImageJ (http://rsb.info.nih.gov/ij/) to measure the area surrounded by thick actin bundles in confocal images. We found that MMC did not reduce the area of tubular structures (Figure 2, A and B), indicating that proliferation is not a crucial event for HPPL to undergo tubular morphogenesis in sandwich culture. MMC inhibited proliferation of HPPL in a separate,

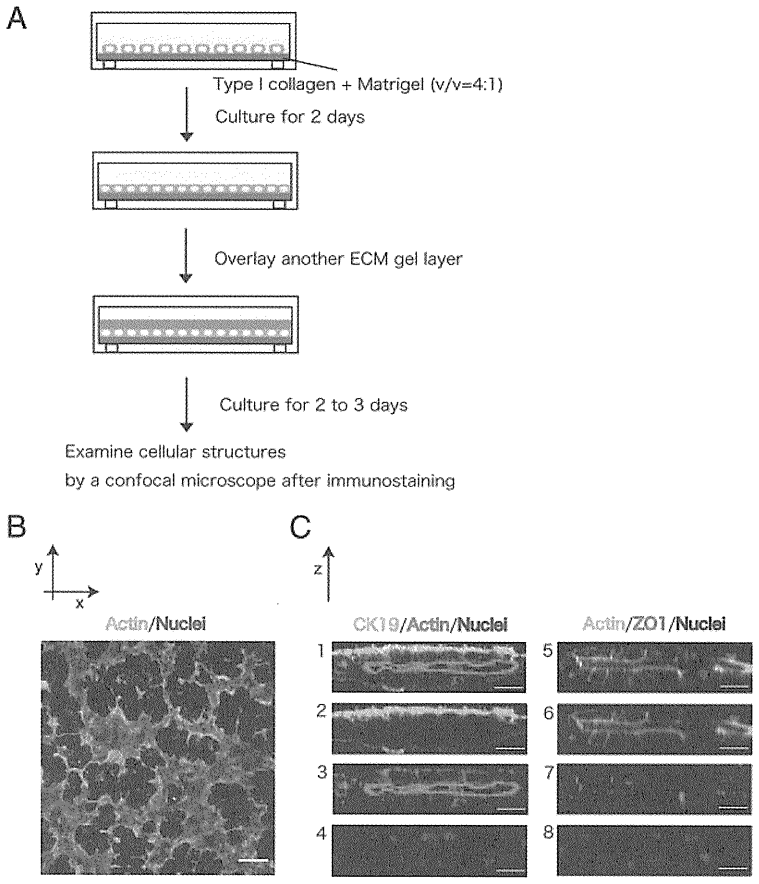

Figure 1. HPPL form tubular structures in sandwich culture. (A) Schematic view of sandwich culture. HPPL were plated on gel containing type I collagen and Matrigel. After HPPL form a monolayer during 2 d of incubation, another layer of gel was overlaid on the monolayer. After additional 2 or 3 d of incubation, cells were fixed and examined with a confocal microscope after immunostaining. (B) A low-magnification image of sandwich culture stained with AlexaFluor 488–conjugated phalloidin and Hoechst34580. A tubular network was visualized as the area surrounded by thick F-actin bundles. Scale bar, 100 μm. (C) Vertical sections of sandwich culture. Cultures were stained with anti-cytokeratin 19 (CK19) antibodies and phalloidin (1–4) or phalloidin and anti-ZO1 antibodies (5–8). CK19$^+$ cells formed the apical lumen surrounded by F-actin bundles. Formation of tight junction was visualized with ZO1 staining. Scale bars, 20 μm.

nonsandwich culture, indicating that the drug worked (Supplementary Figure S1).

Cholangiocytes Do Not Significantly Proliferate during Tubular Morphogenesis In Vivo

Next, we wanted to test whether cholangiocytes in vivo form bile ducts with or without proliferation. To examine the proliferation of cholangiocytes undergoing tubular morphogenesis, we stained frozen sections of E18, postnatal day 0 (P0) and P8 livers with antibodies against CK19 and Ki67, a marker for cells in G1, S, or G2/M phases. In E18 liver, most CK19$^+$ cholangiocytes were negative for Ki67, whereas other liver cells including hepatocytes were positive for Ki67 (Figure 2C). Similarly, in P0 liver, CK19$^+$ cholangiocytes

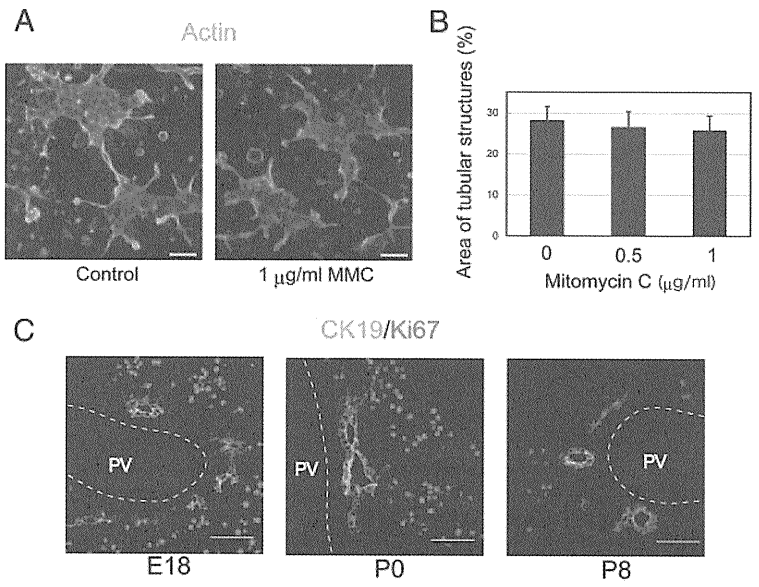

Figure 2. Proliferation is not a crucial event for tubular morphogenesis in vitro and in vivo. (A) Low-magnification images at 2 d after the overlay show tubular structures surrounded by thick F-actin bundles with or without mitomycin C (MMC). MMC, a DNA synthesis inhibitor, was added to culture for 6 h before the overlay. Scale bars, 50 μm. (B) The area of tubular structures in culture was statistically unchanged with or without MMC. The experiment was independently repeated four times. Four fields were selected from each culture and the area of tubular structures in a field was measured using NIH ImageJ after staining with AlexaFluor 488–conjugated phalloidin. (C) Expression of Ki67 in cholangiocytes during bile duct morphogenesis. Frozen sections of embryonic day 18 (E18), postnatal day 0 (P0), and P8 livers were stained with anti-CK19 and anti-Ki67 antibodies. Cells in the parenchyma including hepatocytes were mostly positive for Ki67 in E18 and P0 livers, whereas CK19$^+$ cholangiocytes were mostly negative for Ki67. PV, portal vein. Scale bars, 50 μm.

were negative for Ki67, whereas other cells were still positive for Ki67 (Figure 2C). In P8 liver, both CK19$^+$ cholangiocytes and CK19$^-$ hepatocytes became mostly negative for Ki67 (Figure 2C). These data suggested that cholangiocytes form the tubular structures of bile ducts without significant proliferation in vivo. Thus, we further examined the sandwich culture, where tubular structures were formed without significant proliferation, in order to understand how the monolayer of the ductal plate turns to bile duct tubules.

Tubules Form In Vitro by Cell Migration and Rearrangement

To analyze the process of tubular morphogenesis, we took images of cultures at different time points after the overlay and examined the localization of F-actin bundles and nuclei. See Figure 3A, 1–7: 1, HPPL localized F-actin bundles around the cell cortex in a monolayer; 2, a number of cells lost the apical F-actin bundles (arrowheads), suggesting a loss of apico-basal polarity at 6 h after the overlay; 3, the nucleus of a depolarized cell (an arrowhead) was positioned differently compared with polarized cells, indicating depolarized cells moved up along the Z-axis about 16 h after the overlay; 4 and 5, the number of cells on top of the bottom cell layer increased between 20 and 32 h after the overlay (arrowheads); and 6 and 7, after the second cell layer almost covered the bottom cell layer, the apical luminal space was evident at 48 h and then expanded.

To characterize dynamic stages of morphogenesis with higher spatio-temporal resolution, we further examined the localization of F-actin bundles and β-catenin between 14 and 23 h after the overlay (reconstructed vertical X-Z sections are shown in Figure 3B, 1–10; X-Y sections through the top and bottom of the cell layer are shown in Supplementary Figure S2, A–E). The right side of panels is the edge of the tubular area (panel 1 of Supplementary Figure S2, A–E). Cells in the second layer were first observed only in the right side (panels 1 and 6, closed arrowheads) and then also in the center (panels 2–4 and 7–9, closed arrowheads) and eventually reached to the left side of the image (panels 5 and 10), indicating that cells migrated from the edge to the center of the tubular area. Interestingly, cell–cell contacts shown by β-catenin staining were clear in the bottom cell layer (open arrowheads in panel 6) throughout these time points, but ere less clear between cells in the second layer (an open arrow in panel 6). At 23 h, β-catenin was occasionally observed at cell–cell contact between cells in the second layer (open arrowhead in panel 10). The change of β-catenin localization suggests that intercellular junctions were partly lost during

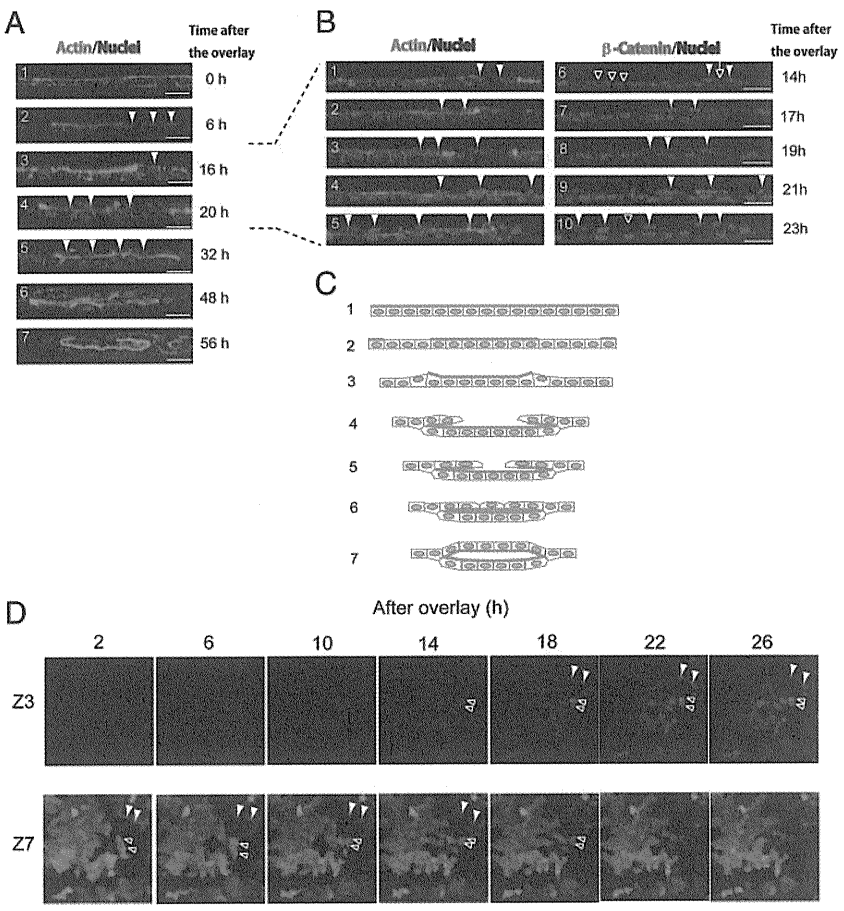

Figure 3. A monolayer of HPPL folds up into tubular structures in sandwich culture. (A) Time course of tubular morphogenesis after the overlay. The overlay of ECM gel on a monolayer of HPPL induced exclusion of F-actin bundles from the apical domain, indicating depolarization of cells (arrowheads in panel 2). Panels 3–5 suggest that depolarized cells first migrated along the Z-axis (an arrowhead in panel 3) and then back along the bottom cell layer (arrowheads in panels 4 and 5). Finally, the apical luminal space was evident at 48 h after the overlay (panel 6) and then expanded (panel 7). X-Y images were taken every 0.7 μm along the Z-axis at each time point using a LSM510 confocal laser scanning microscope and images of a vertical (X-Z) section was reconstructed by using Zeiss LSM software. Scale bars, 20 μm. (B) Time course between 14 and 23 h after the overlay. Cells in the second layer (arrowheads) appeared in the right side of the image (panels 1 and 6) and then were observed also in the center of images (panels 2–4 and 7–9), and eventually reached to the left side (panels 5 and 10). β-Catenin localization at cell–cell contacts were clear between cells in the bottom layer (open arrowheads in panel 6) but not between cells in the second layer (an open arrow in panel 6). Later, β-catenin reappeared at cell–cell contact at 23 h (an open arrowhead in panel 10). X-Y images were taken every 0.5 μm along the Z-axis at each time point using an Olympus FV1000D IX81 confocal laser scanning microscope and images of a vertical (X-Z) section was reconstructed by using Olympus viewer software. Scale bars, 20 μm. (C) On the basis of images at different time points, we propose a model of in vitro tubular morphogenesis in which a monolayer of HPPL folds up into tubular structures. Thick green lines represent F-actin bundles. (D) X-Y images of time-lapse movies between 2 and 26 h after the overlay. HPPL were labeled with GFP. Images at 16 different X-Y planes along the Z-axis were taken in a selected area every 40 min using an Olympus FV1000D IX81 confocal microscope. Panels of the Z7 series show X-Y images of the original monolayer, whereas panels of the Z3 series show a X-Y plane above the monolayer where no cells were initially observed. As indicated by open and closed arrowheads, some cells disappeared from the Z7 plane and instead appeared in the Z3 plane, indicating these cells moved up along the Z-axis.

migration and then were reconstituted around the time when formation of the second layer was almost completed. On the basis of these data, we proposed a model that a monolayer of HPPL folds up into tubular structures (Figure 3C). In this model, depolarized HPPL migrate on a cluster of cells that maintain apico-basal polarity and enclose a volume that eventually becomes the apical luminal space.

The morphogenesis in the model proposed in Figure 3C depends on cell motility. To confirm cellular movement during morphogenesis, we introduced GFP into HPPL to visualize live cells and followed the culture under a confocal microscope. At 2 h after the overlay, we started taking X-Y images at 16 planes along the Z-axis at multiple areas every 40 min. We present movies at the third and seventh X-Y planes, which are, respectively, named Z3 and Z7 planes, of a representative area (Supplementary Movies) and display selected X-Y images from the movies (Figure 3D). HPPL in the original monolayer were followed in the movie of the Z7 plane and panels of selected times from the Z7 series, whereas the area above the monolayer was followed in the movie of the Z3 plane and panels of the Z3 series. As indicated by open and closed arrowheads in Figure 3D, some cells disappeared from the Z7 plane and instead could be observed correspondingly appearing in the Z3 plane. These cellular movements similarly could be observed in the movies of the Z3 and Z7 planes. These data indicate that some of HPPL migrated along the Z-axis during morphogenesis and further support the model shown in Figure 3C.

The PI3K/Akt Pathway Is Essential for Tubular Morphogenesis

We went on to use the sandwich culture system to address the involvement of several important signaling systems in bile duct morphogenesis. It has been shown that PI3K defines the leading edge of cells during migration and the basal domain of epithelial cells during apico-basal polarization (Weiner *et al.*, 2002; Gassama-Diagne *et al.*, 2006; Martin-Belmonte *et al.*, 2007) by producing phosphatidyl-inositide-3,4,5-triphosphate. To test whether the PI3K pathway regulates tubular morphogenesis of HPPL, we first added LY294002, an inhibitor for PI3K, to sandwich cultures at the time of overlay. We found that 20 μM of LY294002 significantly reduced the area of tubular structures (Figure 4A). A similar effect was observed by using wortmannin, another

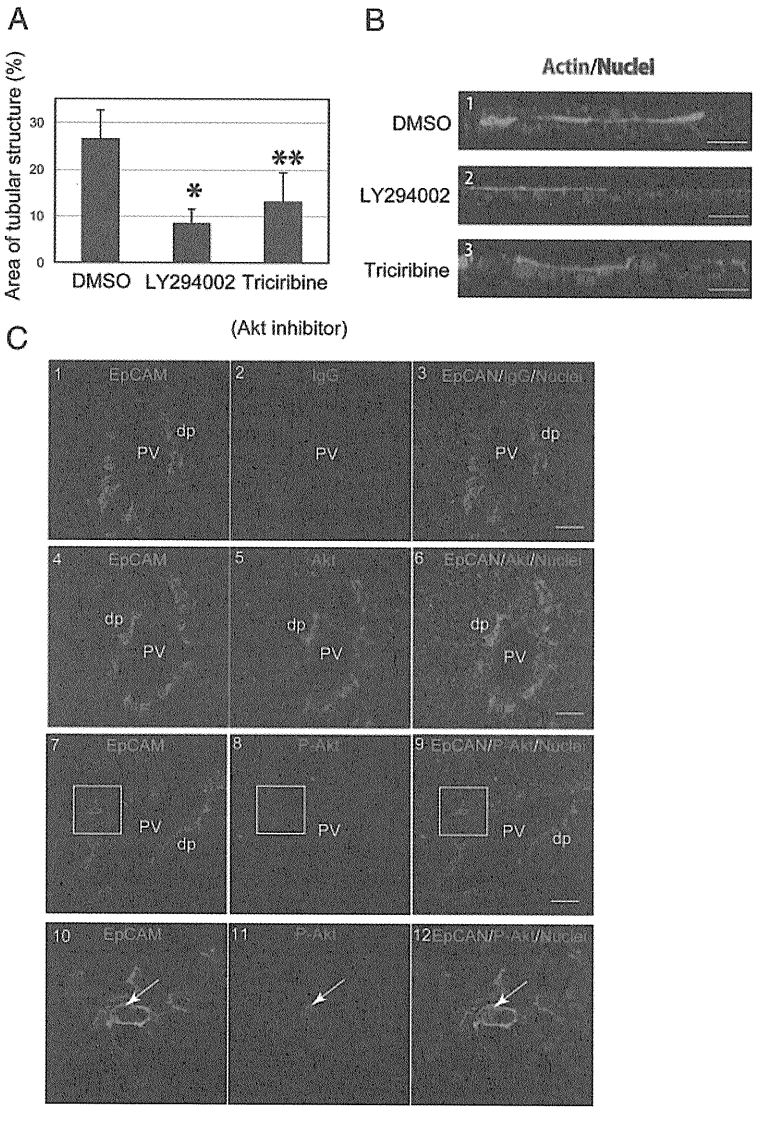

Figure 4. The process of a monolayer of HPPL folding up into tubular structures is regulated by the PI3K/Akt pathway. (A) LY294002, a PI3K inhibitor, or triciribine, an Akt inhibitor, were added to cultures at the time of the overlay. The area of tubular structures was significantly reduced in the presence of LY294002 or triciribine. The culture was independently repeated four times. Four fields were selected from each culture, and areas surrounded by thick F-actin bundles in a field were measured using NIH ImageJ after staining with AlexaFluor 488–conjugated phalloidin. *$p < 0.01$ and **$p < 0.05$, respectively. (B) HPPL formed two cell layers in the control culture at 2 d after the overlay. On the other hand, HPPL remained as a monolayer in the presence of either LY294002 or triciribine. Scale bars, 20 μm. (C) Sections of E18 liver were stained with anti-EpCAM and anti-Akt (panels 4–6) or anti-phospho-Thr308 Akt antibodies (panels 7–12). Boxes in panels 7~9 are enlarged in panels 10–12. As a negative control for Akt and phosho-Thr308 Akt staining, rabbit IgG was used (panels 1–3). Cholangiocytes forming ductal plates (dp) express both EpCAM and Akt (panels 4–6). Furthermore, we found cholangiocytes positive for both EpCAM and phospho-Thr308 Akt (arrows in panels 10–12). PV, portal vein. Scale bars, 50 μm.

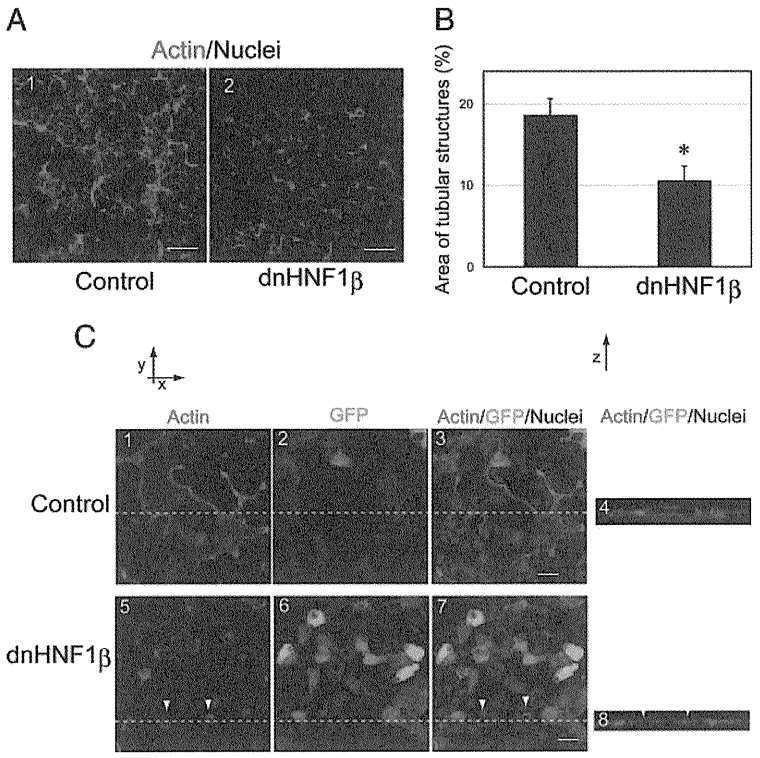

Figure 5. Dominant negative HNF1β inhibits tubular morphogenesis of HPPL. (A) Images at 2 d after the overlay show that tubular structures surrounded by F-actin bundles were observed in the control culture but not in dnHNF1β culture. Scale bars, 100 μm. (B) The area of tubular structures was significantly reduced by overexpression of dnHNF1β. *$p < 0.01$. (C) A large area surrounded by F-actin bundle was observed in a field of the control culture. The X-Z section (panel 4) along the lines in panels 1–3 showed an apical luminal space in the control culture. On the other hand, only tiny areas surrounded by F-actin bundles (arrowheads) were observed in culture overexpressing dnHNF1β (panels 5–8). Retrovirus vector pMXs-dnHNF1β-IRES-GFP was used to express dnHNF1β in HPPL, whereas pMXs-IRES-GFP was used as the control. Scale bars, 20 μm.

PI3K inhibitor (data not shown). Next, we tested whether Akt, a kinase downstream of PI3K, is involved in tubular morphogenesis of HPPL by adding triciribine, an Akt inhibitor. We found that 2 μM of triciribine (a concentration where it is specific for Akt) significantly reduced tubular structures in culture (Figure 4A). Vertical sections of cultures at 48 h after overlay demonstrated that HPPL remained as a monolayer in the presence of LY294002 or triciribine (Figure 4B-2 and 3) whereas HPPL formed a double-cell layer in the control (Figure 4B1). (With triciribine, there was a small amount of upward movement of some nuclei, whereas no such movement was seen with LY294002. The significance of this difference is not clear, but might suggest that Akt is only one of several pathways downstream of PI3K involved in tubular morphogenesis.) These data indicated that the PI3K/Akt pathway is necessary for tubular morphogenesis of HPPL.

To know whether the PI3K/Akt pathway is involved in bile duct morphogenesis in vivo, we prepared sections of E18 liver and examined expression of Akt and phosphorylated Akt in cholangiocytes. We found that Akt was expressed in the periportal area including ductal plates (Figure 4C, 4–6). In addition, we detected signals for phospho-Thr308 Akt on E18 liver sections (Figure 4C, 7–9) and found cholangiocytes positive for phospho-Thr308 Akt (arrows in Figure 4C, 10–12). These data suggest that the PI3K/Akt pathway might be also important for bile duct morphogenesis in vivo.

HNF1β Is Involved in Forming Tubular Structures In Vitro

HNF1β is a transcription factor that is expressed in many tubular structures including bile ducts (Coffinier *et al.*, 1999). Because liver-specific depletion of HNF1β resulted in abnormal formation of intrahepatic bile ducts (Coffinier *et al.*, 2002), HNF1β has been thought to regulate bile duct morphogenesis. To test whether HNF1β regulates tubular morphogenesis of HPPL, we overexpressed HNF1β263fsinGG, a dominant negative form of HNF1β (dnHNF1β; Bai *et al.*, 2002), by using a retrovirus vector, pMXs-dnHNF1β-IRES-GFP. GFP expression indicated that infection efficiency was more than 80%. We compared the area of tubular structures in culture overexpressing dnHNF1β with the control (Figure 5A) and found that dnHNF1β significantly inhibited tubular morphogenesis of HPPL (Figure 5B). We observed normal luminal spaces in the control culture (Figure 5C, 1–4), whereas tiny luminal spaces were observed in cultures overexpressing dnHNF1β (arrowheads in Figure 5B, 5–8). These results indicated that activity of HNF1β is involved in HPPL tubulogenesis in vitro, most likely in enlargement of lumens.

DISCUSSION

We have established a novel organotypic culture system in which HPPL, a mouse liver progenitor cell line, form tubular structures. Using this system, we have demonstrated that depolarized HPPL migrate back along the monolayer, "folding up" to make a double-cell layer. The evidence is that in vertical sections of cultures, F-actin bundles disappeared from the apical domain in a number of cells, and then these depolarized cells were observed on the original cell layer, which eventually formed the second cell layer. After completing formation of the double-cell layer, HPPL generated the apical luminal space between two cell layers.

We recently reported that HPPL embedded as single cells in three-dimensional (3D) ECM gel formed spherical cysts. These cells developed cholangiocyte-type epithelial polarity and acquired secretory functions (Tanimizu *et al.*, 2007). On the other hand, in the present report we observed formation of a tubular network in sandwich culture, where HPPL rearrange the monolayer into tubular structures. These cells

have not fully acquired secretory functions (Supplementary Figure S3). Thus, we consider that we could examine the correlation between epithelial polarization and functional differentiation (secretory function) of liver progenitor cells along the cholangiocyte lineage in 3D cyst culture, whereas we could analyze the process of tubular morphogenesis of bile ducts in sandwich culture. By combining the two approaches we will be able to understand the molecular mechanisms governing bile duct morphogenesis. Recently, Hashimoto *et al.* (2008) reported mature cholangiocytes isolated from adult rat formed tubular structures in collagen overlay culture. They showed transport of fluorescein diacetate into the apical luminal space, which we could not observe. Those authors did not, however, examine the mechanisms of cell movement or signaling pathways involved in tubular morphogenesis. A further advantage of our system is that we used liver progenitor cells rather than mature cholangiocytes and therefore, we could more directly study the developmental process of bile duct formation.

Bile duct morphogenesis in vivo can be divided into three distinct stages: formation of a double-cell layer, generation of the apical luminal space, and reorganization of the ductal plate along with the luminal space into tubules. Our results that a monolayer of HPPL folds up into a tubular structure have demonstrated a possible pathway of bile duct morphogenesis, in particular a potential mechanism for the first step. At least three major types of nonmutually exclusive models can be envisioned as to how the initial monolayer of cells in a ductal plate can be converted to a double layer of cells in vivo (Figure 6). In model 1, cells in the monolayer of the plate divide, forming a second layer. In model 2, certain hepatoblasts in the adjacent parenchyma differentiate into cholangiocytes and form the second layer of the plate. In model 3, which best fits the morphogenesis of HPPL in sandwich culture, some cells in the initial monolayer rearrange themselves by moving on top of the original monolayer, thereby forming the second layer.

Model 1 relies on proliferation of cells in the ductal plate to form the double layer. However, as we observed that proliferation is dramatically reduced when hepatoblasts differentiate to cholangiocytes, duplication of a single-cell layer by proliferation is not likely to be a major process in generating a double-cell layer in vivo. On the other hand, models 2 and 3, respectively, rely on recruitment of cells from outside the monolayer and migration of cells in the ductal plate to form the double layer. Thus, in both cases, proliferation of hepatoblasts is not necessary to form the second layer and these models of in vivo bile duct morphogenesis seem more likely compared with model 1.

In model 2, certain hepatoblasts next to the first layer of cholangiocytes differentiate to cholangiocytes, which form the second layer of the ductal plate. In support of this model, recent reports indicate that activin/TGFβ signaling is activated more strongly in hepatoblasts near the portal vein than those in the parenchyma of fetal liver and thereby induces cholangiocyte differentiation of hepatoblasts only near the portal vein (Clotman *et al.*, 2005). In the model where cholangiocyte differentiation is induced outside of the first layer of the ductal plate, the activin/TGFβ signaling pathway may be preferable to the Notch signaling pathway, which also induces cholangiocytes from hepatoblasts (McCright *et al.*, 2002; Tanimizu and Miyajima, 2004). In contrast

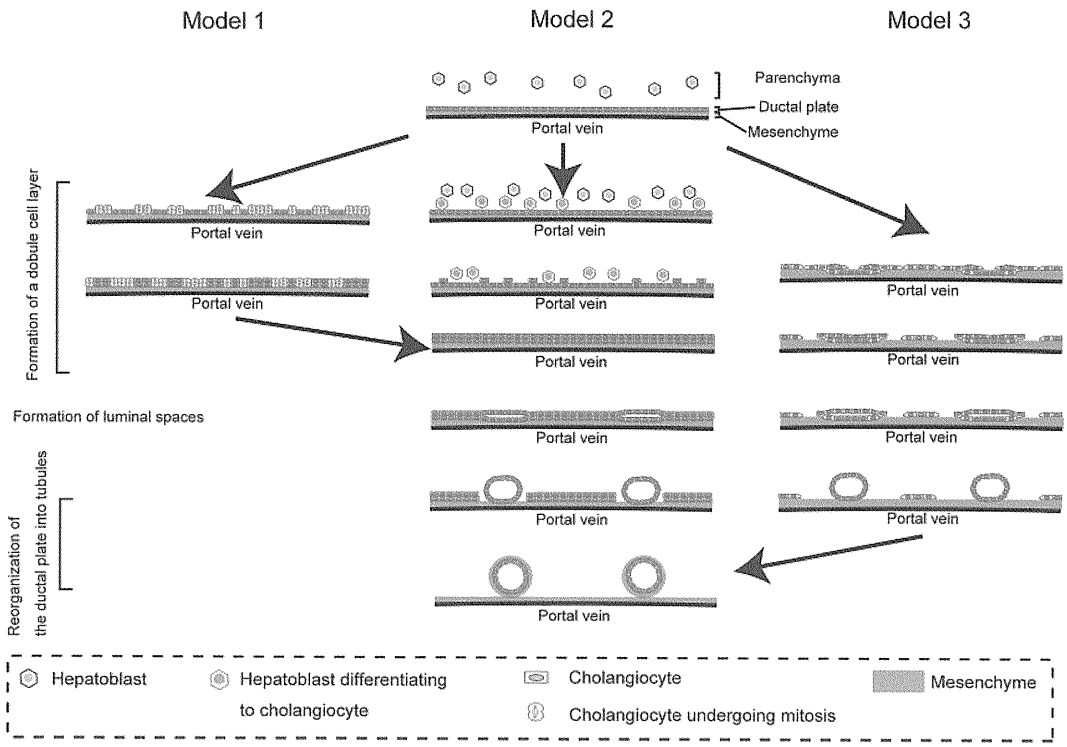

Figure 6. Three possible models for bile duct morphogenesis. Bile duct morphogenesis starts from a single layer of cholangiocyte called the ductal plate around the portal vein. To form a double-cell layer, we considered three possible models. Cholangiocytes proliferate to generate the second layer of the ductal plate (model 1), hepatoblasts outside the first layer are induced to differentiate to cholangiocytes (model 2), or cholangiocytes fold up to form a double layer (model 3). After luminal space is generated between the two cell layers, the ductal plate is reorganized into tubular structures. During this stage, small, flat luminal spaces are enlarged and become round. Cholangiocytes that remain in the ductal plate eventually disappear.

to the Notch pathway, which requires direct interaction between Jagged1$^+$ periportal cells and Notch2$^+$ hepatoblasts to induce cholangiocyte differentiation of hepatoblasts, the activin/TGFβ signal can be activated without direct cell–cell interaction.

During tubular morphogenesis in some types of epithelial structures, such as mammary acini, cell death is important for creation of the luminal space (Debnath and Brugge, 2005). In the case of bile duct morphogenesis, apoptotic cell death might be an important event during rearrangement of the ductal plate (Terada and Nakanuma, 1995; Sergi *et al.*, 2000). Given that each portal vein is usually associated with one or two bile ducts, only part of the cholangiocytes that form the ductal plate develop into tubular structures. Other cholangiocytes that remain in the ductal plate gradually regress. If bile duct morphogenesis proceeds via model 1 or 2, a significant number of cells would remain in the ductal plate, which would be eliminated later. However, apoptotic cholangiocytes were not frequently observed in mouse liver at E18, P5, and P10 (Supplementary Figure S4). In contrast, many cells would be predicted to leave the ductal plate to form the second layer during tubulogenesis, and fewer cells need to be eliminated by apoptosis, if morphogenesis proceeds via model 3.

In our sandwich culture, no pool of progenitor cells that could differentiate to cholangiocytes and be recruited to form a second layer was present, yet a second layer was formed. This indicates that it is at least possible for double layer to form without recruitment of outside cells. In addition, the result that cholangiocytes do not frequently die by apoptosis (Supplementary Figure S4) is consistent with model 3. On the other hand, the previously reported in vivo evidence that activin/TGFβ signaling involved in bile duct development is supportive of model 2. Thus, although model 1 seems unlikely in light of our data, we cannot determine whether model 2 or 3 are better able to explain bile duct morphogenesis in vivo. It is of course possible that both models 2 and 3 may occur during bile duct development in vivo.

The process of folding up a monolayer can be segregated into three steps: the first step is loss of apico-basal polarity, the second is migration of depolarized cells, and the third is expansion of the apical luminal space. Morphogenesis was completely blocked by inhibiting PI3K. So far, we cannot tell whether PI3K is only necessary for the first step or also needed for later steps. However, because Akt was constitutively phosphorylated during the process of folding up (data not shown), it is tempting to speculate the PI3K/Akt pathway is involved in all three steps. Morphogenesis was also decreased by reducing the activity of HNF1β, though the nature of the effect was quite different from blocking the PI3K/Akt pathway. In cultures with dnHNF1β, F-actin in the apical domain disappeared and only much smaller lumens were observed. (In contrast, apical F-actin remained in cultures with LY294002 and triciribine.) This suggests that transcriptional activity of HNF1β is necessary for HPPL to expand the apical luminal space, but not to undergo the initial event where they depolarize before starting migration. This illustrates how different molecular pathways are involved in distinct steps in tubulogenesis.

In vivo, folding of a monolayer to produce a tube has been described during formation of the neural tube (Zohn *et al.*, 2003). In this case, a single lumen is produced. In contrast during formation of bile ducts, multiple lumens are generated and these rearrange to eventually produce a branching tubular network of bile ducts. As far as we know, this type of process does not occur normally during development of other epithelial organs, e.g., kidney or lung. Even though tubular morphogenesis in different organs utilizes apparently distinct mechanisms, many of the same molecules such as PI3K/Akt and HNF1β have been implicated in formation of a variety of tubular structures (Coffinier *et al.*, 2002; Tang *et al.*, 2002; Liu *et al.*, 2004; Lebrun *et al.*, 2005; Kim and Dressler, 2007). This suggests that there may be common principles of tubulogenesis that underlie seemingly diverse mechanisms of tubulogenesis. Using in vitro organotypic culture systems, we can access molecular mechanisms of morphogenetic processes in detail help us to find out common principles of tubular morphogenesis during organogenesis (Ojakian *et al.*, 2001; Yu *et al.*, 2003; Zegers *et al.*, 2003; Walid *et al.*, 2008).

In summary, using our newly developed sandwich culture system, we found that HPPL folds a monolayer up to make a double-cell layer and then form tubular structures. This is an unusual (possibly unique) and interesting variation on known mechanisms for tubule formation in various organs. In addition, because tubulogenesis in the culture seems very similar to in vivo bile duct morphogenesis, our sandwich culture system of liver progenitor cells is likely to prove useful in understanding abnormal bile duct morphogenetic processes such as ductal plate malformation.

ACKNOWLEDGMENTS

We thank the members of the Mostov and Miyajima laboratories for helpful discussions. N.T. was supported by a Pilot/Feasibility funding from the Liver Center of University of California San Francisco. This work was supported by grants from the National Institutes of Health to K.E.M. and by a research grant from the Ministry of Education, Sports, Science, and Technology, Japan, to N.T.

REFERENCES

Bai, Y., Pontoglio, M., Hiesberger, T., Sinclair, A. M., and Igarashi, P. (2002). Regulation of kidney-specific Ksp-cadherin gene promoter by hepatocyte nuclear factor-1beta. Am. J. Physiol. Renal. Physiol. *283*, F839–F851.

Bryant, D. M., and Mostov, K. E. (2008). From cells to organs: building polarized tissue. Nat. Rev. Mol. Cell Biol. *9*, 887–901.

Clotman, F., Jacquemin, P., Plumb-Rudewiez, N., Pierreux, C. E., Van der Smissen, P., Dietz, H. C., Courtoy, P. J., Rousseau, G. G., and Lemaigre, F. P. (2005). Control of liver cell fate decision by a gradient of TGF beta signaling modulated by Onecut transcription factors. Genes Dev. *19*, 1849–1854.

Coffinier, C., Barra, J., Babinet, C., and Yaniv, M. (1999). Expression of the vHNF1/HNF1beta homeoprotein gene during mouse organogenesis. Mech. Dev. *89*, 211–213.

Coffinier, C., Gresh, L., Fiette, L., Tronche, F., Schutz, G., Babinet, C., Pontoglio, M., Yaniv, M., and Barra, J. (2002). Bile system morphogenesis defects and liver dysfunction upon targeted deletion of HNF1beta. Development *129*, 1829–1838.

Crawford, J. M. (2002). Development of the intrahepatic biliary tree. Semin. Liver Dis. *22*, 213–226.

Debnath, J., and Brugge, J. S. (2005). Modelling glandular epithelial cancers in three-dimensional cultures. Nature Rev. *5*, 675–688.

Fitz, J. G. (2002). Regulation of cholangiocyte secretion. Semin. Liver Dis. *22*, 241–249.

Gassama-Diagne, A., Yu, W., ter Beest, M., Martin-Belmonte, F., Kierbel, A., Engel, J., and Mostov, K. (2006). Phosphatidylinositol-3,4,5-trisphosphate regulates the formation of the basolateral plasma membrane in epithelial cells. Nat. Cell Biol. *8*, 963–970.

Hall, H. G., Farson, D. A., and Bissell, M. J. (1982). Lumen formation by epithelial cell lines in response to collagen overlay: a morphogenetic model in culture. Proc. Natl. Acad. Sci. USA *79*, 4672–4676.

Hashimoto, W., Sudo, R., Fukasawa, K., Ikeda, M., Mitaka, T., and Tanishita, K. (2008). Ductular network formation by rat biliary epithelial cells in the dynamical culture with collagen gel and dimethylsulfoxide stimulation. American J. Pathol. *173*, 494–506.

Hogan, B. L., and Kolodziej, P. A. (2002). Organogenesis: molecular mechanisms of tubulogenesis. Nat. Rev. Genet. *3*, 513–523.

Hunter, M. P., Wilson, C. M., Jiang, X., Cong, R., Vasavada, H., Kaestner, K. H., and Bogue, C. W. (2007). The homeobox gene Hhex is essential for proper hepatoblast differentiation and bile duct morphogenesis. Dev. Biol. *308*, 355–367.

Kim, D., and Dressler, G. R. (2007). PTEN modulates GDNF/RET mediated chemotaxis and branching morphogenesis in the developing kidney. Dev. Biol. *307*, 290–299.

Kodama, Y., Hijikata, M., Kageyama, R., Shimotohno, K., and Chiba, T. (2004). The role of notch signaling in the development of intrahepatic bile ducts. Gastroenterology *127*, 1775–1786.

Lebrun, G., Vasiliu, V., Bellanne-Chantelot, C., Bensman, A., Ulinski, T., Chretien, Y., and Grunfeld, J. P. (2005). Cystic kidney disease, chromophobe renal cell carcinoma and TCF2 (HNF1 beta) mutations. Nat. Clin. Pract. Nephrol. *1*, 115–119.

Lemaigre, F. P. (2003). Development of the biliary tract. Mech. Dev. *120*, 81–87.

Liu, J., Nethery, D., and Kern, J. A. (2004). Neuregulin-1 induces branching morphogenesis in the developing lung through a P13K signal pathway. Experimental lung Res. *30*, 465–478.

Low, Y., Vijayan, V., and Tan, C. E. (2001). The prognostic value of ductal plate malformation and other histologic parameters in biliary atresia: an immunohistochemical study. J. Pediatr.*139*, 320–322.

Lubarsky, B., and Krasnow, M. A. (2003). Tube morphogenesis: making and shaping biological tubes. Cell *112*, 19–28.

Martin-Belmonte, F., Gassama, A., Datta, A., Yu, W., Rescher, U., Gerke, V., and Mostov, K. (2007). PTEN-mediated apical segregation of phosphoinositides controls epithelial morphogenesis through Cdc42. Cell *128*, 383–397.

McCright, B., Lozier, J., and Gridley, T. (2002). A mouse model of Alagille syndrome: Notch2 as a genetic modifier of Jag1 haploinsufficiency. Development *129*, 1075–1082.

O'Brien, L. E., Yu, W., Tang, K., Jou, T. S., Zegers, M. M., and Mostov, K. E. (2006). Morphological and biochemical analysis of Rac1 in three-dimensional epithelial cell cultures. Methods Enzymol. *406*, 676–691.

Ojakian, G. K., Ratcliffe, D. R., and Schwimmer, R. (2001). Integrin regulation of cell-cell adhesion during epithelial tubule formation. J. Cell Sci. *114*, 941–952.

Ojakian, G. K., and Schwimmer, R. (1994). Regulation of epithelial cell surface polarity reversal by beta 1 integrins. J. Cell Sci. *107*(Pt 3), 561–576.

Paumgartner, G. (2006). Medical treatment of cholestatic liver diseases: From pathobiology to pharmacological targets. World J. Gastroenterol. *12*, 4445–4451.

Schmucker, D. L., Ohta, M., Kanai, S., Sato, Y., and Kitani, K. (1990). Hepatic injury induced by bile salts: correlation between biochemical and morphological events. Hepatology *12*, 1216–1221.

Sergi, C., Adam, S., Kahl, P., and Otto, H. F. (2000). Study of the malformation of ductal plate of the liver in Meckel syndrome and review of other syndromes presenting with this anomaly. Pediatr. Dev. Pathol. *3*, 568–583.

Tan, C. E., Chan, V. S., Yong, R. Y., Vijayan, V., Tan, W. L., Fook Chong, S. M., Ho, J. M., and Cheng, H. H. (1995). Distortion in TGF beta 1 peptide immunolocalization in biliary atresia: comparison with the normal pattern in the developing human intrahepatic bile duct system. Pathol. Int. *45*, 815–824.

Tang, M. J., Cai, Y., Tsai, S. J., Wang, Y. K., and Dressler, G. R. (2002). Ureteric bud outgrowth in response to RET activation is mediated by phosphatidylinositol 3-kinase. Dev. Biol. *243*, 128–136.

Tanimizu, N., and Miyajima, A. (2004). Notch signaling controls hepatoblast differentiation by altering the expression of liver-enriched transcription factors. J. Cell Sci. *117*, 3165–3174.

Tanimizu, N., Miyajima, A., and Mostov, K. E. (2007). Liver progenitor cells develop cholangiocyte-type epithelial polarity in three-dimensional culture. Mol. Biol. Cell *18*, 1472–1479.

Tanimizu, N., Nishikawa, M., Saito, H., Tsujimura, T., and Miyajima, A. (2003). Isolation of hepatoblasts based on the expression of Dlk/Pref-1. J. Cell Sci. *116*, 1775–1786.

Tanimizu, N., Saito, H., Mostov, K., and Miyajima, A. (2004). Long-term culture of hepatic progenitors derived from mouse Dlk+ hepatoblasts. J. Cell Sci. *117*, 6425–6434.

Terada, T., and Nakanuma, Y. (1995). Detection of apoptosis and expression of apoptosis-related proteins during human intrahepatic bile duct development. Am. J. Pathol. *146*, 67–74.

Walid, S., Eisen, R., Ratcliffe, D. R., Dai, K., Hussain, M. M., and Ojakian, G. K. (2008). The PI 3-kinase and mTOR signaling pathways are important modulators of epithelial tubule formation. J. Cell. Physiol. *216*, 469–479.

Weiner, O. D., Neilsen, P. O., Prestwich, G. D., Kirschner, M. W., Cantley, L. C., and Bourne, H. R. (2002). A PtdInsP(3)- and Rho GTPase-mediated positive feedback loop regulates neutrophil polarity. Nat. Cell Biol. *4*, 509–513.

Yoon, J. H., and Gores, G. J. (2002). Death receptor-mediated apoptosis and the liver. J. Hepatol. *37*, 400–410.

Yu, W., O'Brien, L. E., Wang, F., Bourne, H., Mostov, K. E., and Zegers, M. M. (2003). Hepatocyte growth factor switches orientation of polarity and mode of movement during morphogenesis of multicellular epithelial structures. Mol. Biol. Cell *14*, 748–763.

Zegers, M. M., O'Brien, L. E., Yu, W., Datta, A., and Mostov, K. E. (2003). Epithelial polarity and tubulogenesis in vitro. Trends Cell Biol. *13*, 169–176.

Zohn, I. E., Chesnutt, C. R., and Niswander, L. (2003). Cell polarity pathways converge and extend to regulate neural tube closure. Trends Cell Biol. *13*, 451–454.

Zuk, A., and Matlin, K. S. (1996). Apical beta 1 integrin in polarized MDCK cells mediates tubulocyst formation in response to type I collagen overlay. J. Cell Sci. *109*(Pt 7), 1875–1889.

MECHANISMS OF DEVELOPMENT 126 (2009) 665–676

available at www.sciencedirect.com

ScienceDirect

journal homepage: www.elsevier.com/locate/modo

Mouse hepatoblasts at distinct developmental stages are characterized by expression of EpCAM and DLK1: Drastic change of EpCAM expression during liver development

Minoru Tanaka[a,b,*,1], *Mayuko Okabe*[a,1], *Kaori Suzuki*[a,1], *Yoshiko Kamiya*[a,b], *Yuko Tsukahara*[a], *Shigeru Saito*[a], *Atsushi Miyajima*[a]

[a]*Institute of Molecular and Cellular Biosciences, The University of Tokyo, 1-1-1 Yayoi, Tokyo 113-0032, Japan*
[b]*Promotion of Independence for Young Investigators of Japan Science and Technology Agency (JST), Japan*

ARTICLE INFO

Article history:
Received 27 September 2008
Received in revised form
29 May 2009
Accepted 6 June 2009
Available online 13 June 2009

Keywords:
Mouse
Hepatoblasts
EpCAM
DLK1
Hepatocyte
Cholangiocyte
Bile duct
Flow cytometry

ABSTRACT

Hepatoblasts are hepatic progenitor cells that expand and give rise to either hepatocyte or cholangiocytes during liver development. We previously reported that delta-like 1 homolog (DLK1) is expressed in the mouse liver primordium at embryonic day (E) 10.5 and that DLK1$^+$ cells in E14.5 liver contain high proliferative and bipotential hepatoblasts. While the expression of epithelial cell adhesion molecule (EpCAM) in hepatic stem/progenitor cells has been reported, its expression profile at an early stage of liver development remains unknown. In this study, we show that EpCAM is expressed in mouse liver bud at E9.5 and that EpCAM$^+$DLK1$^+$ hepatoblasts form hepatic cords at the early stage of hepatogenesis. DLK1$^+$ cells of E11.5 liver were fractionated into EpCAM$^+$ and EpCAM$^-$ cells; one forth of EpCAM$^+$DLK1$^+$ cells formed a colony in vitro whereas EpCAM$^-$DLK1$^+$ cells rarely did it. Moreover, EpCAM$^+$DLK1$^+$ cells contained cells capable of forming a large colony, indicating that EpCAM$^+$DLK1$^+$ cells in E11.5 liver contain early hepatoblasts with high proliferation potential. Interestingly, EpCAM expression in hepatoblasts was dramatically reduced along with liver development and the colony-forming capacities of both EpCAM$^+$DLK1$^+$ and EpCAM$^-$DLK1$^+$ cells were comparable in E14.5 liver. It strongly suggested that most of mouse hepatoblasts are losing EpCAM expression at this stage. Moreover, we provide evidence that EpCAM$^+$DLK1$^+$ cells in E11.5 liver contain extrahepatic bile duct cells as well as hepatoblasts, while EpCAM$^-$DLK1$^+$ cells contain mesothelial cell precursors. Thus, the expression of EpCAM and DLK1 suggests the developmental pathways of mouse liver progenitors.

1. Introduction

Liver development begins at embryonic day (E) 8.5 in the mouse from the foregut endoderm. The ventral wall of the foregut endoderm faces the developing heart by approximately E8 and receives inductive signals for the hepatic fate, such as fibroblast growth factor (FGF), from the heart (Douarin, 1975; Gualdi et al., 1996; Jung et al., 1999). Septum transversum mesenchyme (STM) also contributes to liver development from the foregut endoderm by providing bone

* *Corresponding author.* Address: Institute of Molecular and Cellular Biosciences, The University of Tokyo, 1-1-1 Yayoi, Tokyo 113-0032, Japan. Tel.: +81 3 5841 7889; fax: +81 3 5841 8475.
E-mail address: tanaka@iam.u-tokyo.ac.jp (M. Tanaka).
[1] These authors contributed equally to this study.
0925-4773/$ - see front matter © 2009 Elsevier Ireland Ltd. All rights reserved.
doi:10.1016/j.mod.2009.06.939